



1 **Modelling soil CO₂ production and transport with dynamic source and diffusion terms:**

2 **Testing the steady-state assumption using DETECT v1.0**

3

4 Edmund Ryan^{1,2*}, Kiona Ogle^{2,3,4,5}, Heather Kropp⁶, Kimberly E. Samuels-Crow³,

5 Yolima Carrillo⁷, Elise Pendall⁷

6 ¹Lancaster Environment Centre, Lancaster University, Lancaster, UK

7 ²School of Life Sciences, Arizona State University, Tempe, Arizona, USA

8 ³School of Informatics, Computing, and Cyber Systems, Northern Arizona University, Flagstaff,

9 Arizona, USA

10 ⁴Center for Ecosystem Science and Society, Northern Arizona University, Flagstaff, Arizona,

11 USA

12 ⁵Department of Biological Sciences, Northern Arizona University, Flagstaff, Arizona, USA

13 ⁶Department of Geography, Colgate University, Hamilton, NY, USA

14 ⁷Hawkesbury Institute for the Environment, Western Sydney University, NSW, Australia

15 *Corresponding author:

16 Lancaster Environment Centre,

17 Lancaster,

18 Lancashire. LA1 4YW

19 United Kingdom.

20 Tel: +44 (0)1524 594009

21 Email: edmund.ryan@lancaster.ac.uk

22



23 Abstract

24 The flux of CO₂ from the soil to the atmosphere (soil respiration, R_{soil}) is a major component of
25 the global carbon cycle. Methods to measure and model R_{soil} , or partition it into different
26 components, often rely on the assumption that soil CO₂ concentrations and fluxes are in steady
27 state, implying that R_{soil} is equal to the rate at which CO₂ is produced by soil microbial and root
28 respiration. Recent research, however, questions the validity of this assumption. Thus, the aim
29 of this work was two-fold: (1) to describe a non-steady state (NSS) soil CO₂ transport and
30 production model, DETECT, and (2) to use this model to evaluate the environmental conditions
31 under which R_{soil} and CO₂ production are likely in NSS. The backbone of DETECT is a non-
32 homogeneous, partial differential equation (PDE) that describes production and transport of soil
33 CO₂, which we solve numerically at fine spatial and temporal resolution (e.g., 0.01 m increments
34 to 1 m, every 6 hours). Production of soil CO₂ is simulated for every depth and time increment as
35 the sum of root respiration and microbial decomposition of soil organic matter, both of which
36 can be driven by current and antecedent soil water content and temperature, which can also vary
37 by time and depth. We also analytically solved the ordinary differential equation (ODE)
38 corresponding to the steady-state (SS) solution to the PDE model. We applied the DETECT NSS
39 and SS models to the 6-month growing season period representative of a native grassland in
40 Wyoming. Simulation experiments were conducted with both model versions to evaluate factors
41 that could affect departure from SS: (1) varying soil texture; (2) shifting the timing or frequency
42 of precipitation; and (3) with and without the environmental antecedent drivers. For a coarse-
43 textured soil, R_{soil} from the SS model closely matched that of the NSS model. However, in a
44 fine-textured (clay) soil, growing season R_{soil} was ~3% higher under the assumption of NSS
45 (versus SS). These differences were exaggerated in clay soil at daily time-scales whereby R_{soil}



46 under the SS assumption deviated from NSS by up to ~20% in the 10 days following a major
47 precipitation event. Moreover, incorporation of antecedent drivers increased the magnitude of
48 R_{soil} by 15% to 37% for coarse- and fine-textured soils, respectively. However, the responses of
49 R_{soil} to the timing of precipitation and antecedent drivers did not differ between SS and NSS
50 assumptions. In summary, the assumption of SS conditions can be violated depending on soil
51 type and soil moisture status, as affected by precipitation inputs, and the DETECT model
52 provides a framework for accommodating NSS conditions to better predict R_{soil} and associated
53 soil carbon cycling processes.

54 *Keywords:* antecedent soil water content, DETECT, diffusion model, modelling soil CO₂, non-
55 steady-state, precipitation frequency, soil respiration, soil texture, steady-state.

56



1 Introduction

2 The flux of CO₂ to the atmosphere from the soil (i.e., soil respiration, R_{soil}) is one of the largest
3 fluxes in the global C cycle and is approximately ten times the annual amount of CO₂ emitted by
4 fossil fuel burning (Friedlingstein et al., 2014; Hashimoto et al., 2015). Moreover, global change
5 experiments and predictions from models agree that R_{soil} is expected to increase in a future
6 climate of elevated CO₂ and warming (Cox, 2001; Davidson and Janssens, 2006; Pendall et al.,
7 2013; Piao et al., 2009; Ryan et al., 2015). Therefore, monitoring R_{soil} is important for
8 quantifying and modeling the global C cycle.

9 Commonly, R_{soil} is monitored by directly measuring surface soil CO₂ fluxes using various
10 chamber methods (Luo and Zhou, 2010; Risk et al., 2011) or by estimating R_{soil} from soil CO₂
11 concentrations measured at multiple depths using probe methods (Pendall et al., 2003; Tang et
12 al., 2003; Vargas et al., 2010). The probe methods employ diffusion equations that often rely on
13 the assumption that R_{soil} at the surface is in steady state (SS) with subsurface CO₂ production by
14 roots and micro-organisms (Baldocchi et al., 2006; Lee et al., 2004; Luo and Zhou, 2010;
15 Šimůnek et al., 2012; Tang et al., 2003; Vargas et al., 2010). That is, the SS assumption
16 essentially assumes that CO₂ produced by roots and microbes within the soil profile is
17 instantaneously respired from the soil surface, effectively neglecting delays due to CO₂ transport
18 times. Partitioning R_{soil} (surface flux) into its different components (e.g., sub-surface
19 heterotrophic [microbes] versus autotrophic [root or rhizosphere] respiration) using isotope
20 methods (Hui and Luo, 2004; Ogle and Pendall, 2015), trenching methods (Šimůnek and Suarez,
21 1993), or soil CO₂ models (Vargas et al., 2010) also relies on the SS assumption. Even
22 simulations of the vertical movement of soil CO₂ through snow have employed a SS diffusion
23 model (Monson et al. 2006). Recent work, however, calls into question whether this SS



1 assumption is valid most of the time or in most systems (Maggi and Riley, 2009; Nickerson and
2 Risk, 2009).

3 Given the use of the SS assumption in a diverse range of settings, the aim of this study
4 was to determine the meteorological and site specific conditions under which the SS assumption
5 is valid, and the circumstances under which a non-steady state (NSS) model substantially
6 improves our understanding of subsurface processes that lead to observed R_{soil} . We focused on
7 soil texture because it is a critical factor underlying soil porosity and tortuosity, which, in turn,
8 control soil CO₂ diffusion rates (Bouma and Bryla, 2000). For example, coarse (e.g., high sand
9 content) soils generally facilitate fast diffusion rates, especially under low soil moisture
10 conditions associated with high air-filled porosity (Bouma and Bryla, 2000); the opposite is
11 expected for finer-grained (e.g., silt or clay) soils. Thus, we expected coarse soils to generally
12 induce SS conditions for soil CO₂, whereas fine-grained soils would likely produce frequent and
13 longer duration NSS conditions, especially following rain pulses that decrease air-filled porosity,
14 thereby reducing CO₂ diffusivity.

15 We also focused on the impacts of precipitation variability given that the timing and
16 magnitude of precipitation pulses can have large effects on R_{soil} (Borken and Matzner, 2009;
17 Cable et al., 2008; Huxman et al., 2004; Ogle et al., 2015; Schwinning et al., 2004; Sponseller,
18 2007). Precipitation indirectly impacts R_{soil} via its influence on soil moisture dynamics, and soil
19 moisture and soil texture affect both diffusivity (physical process) and CO₂ production (primarily
20 biological process governed by roots and microbes). Moreover, as precipitation pulses infiltrate
21 the soil, filling of pore spaces with water can result in a displacement of CO₂, which may be seen
22 as a transient spike in R_{soil} (e.g., Lee et al., 2004). Such transient spikes, however, may also be
23 attributable to changes in decomposition, microbial growth, and/or C substrate availability in



1 response to wetting (Birch, 1958; Borken et al., 2003; Jarvis et al., 2007; Meisner et al., 2013;
2 Xiang et al., 2008). This transient response may be followed by a depression in R_{soil} since water-
3 filled pores will ultimately slow CO_2 diffusion and transport (Bouma and Bryla, 2000). These
4 linked effects imply that precipitation pulses and their effects on soil moisture are likely to
5 impose NSS soil CO_2 conditions, but the manner in which such pulses impact these processes is
6 temporally dynamic and spatially complex, and therefore difficult to measure directly.

7 We evaluated the importance of soil texture and precipitation variability on SS versus
8 NSS soil CO_2 behavior via a simulation-based approach. To allow for the possibility of both SS
9 and NSS behavior, we implemented a depth- and time-varying CO_2 transport and production
10 model that builds on the groundbreaking work of Fang and Moncrieff (1999), Hui and Luo
11 (2004), Nickerson and Risk (2009), Moyes et al. (2010) and Risk et al. (2012). These processes
12 are captured by a partial differential equation (PDE) model that is grounded in diffusion theory,
13 and solved numerically. Some current NSS models make simplifying assumptions such as
14 assuming depth-invariant production rates (e.g., Fang and Moncrieff, 1999), or assuming that
15 production only responds to concurrent environmental conditions (e.g., Nickerson and Risk,
16 2009). Such simplifications may make it difficult to evaluate physical and biological conditions
17 leading to SS versus NSS behavior.

18 We addressed the aforementioned shortcomings of existing NSS models with the
19 DETECT (DEconvolution of Temporally varying Ecosystem Carbon componenTs) model,
20 version 1.0 (v1.0), which implemented four improvements. First, we simulated soil CO_2 at 0.01
21 m increments—from the surface to a depth of 1 m—to ensure numerical accuracy of the
22 solutions (Haberman, 1998). Second, we drove the PDE model with output from a dynamic,
23 physically-based model of soil water and temperature in porous media (HYDRUS; Simunek et



1 al., 2005; Šimůnek et al., 2008) that predicts sub-daily soil environmental conditions in each 0.01
2 m increment. Third, we simulated the production of CO₂ by microbial and root respiration in
3 each increment by linking these processes to the depth-specific soil conditions using existing
4 respiration models that are typically applied to “bulk” soil (Cable et al., 2008; Davidson et al.,
5 2012; Lloyd and Taylor, 1994; Todd-Brown et al., 2012). Fourth, a growing body of evidence
6 suggests that antecedent or past environmental or meteorological conditions are important for
7 predicting soil and ecosystem CO₂ fluxes (Barron-Gafford et al., 2014; Cable et al., 2013; Ryan
8 et al., 2015), and we accounted for these antecedent effects in the respiration (or production)
9 submodels. For example, observed increases in ecosystem and soil respiration rates after a rain
10 event are generally greater if the rain event occurs during a dry period compared to a wet period
11 (Cable et al., 2013; Cable et al., 2008; Sponseller, 2007; Thomas et al., 2008; Xu et al., 2004).
12 Such antecedent effects may underlie the importance of biological versus physical processes in
13 governing the transition between SS and NSS behavior.

14 After describing the DETECT model, we subsequently use it to explore the effects of soil
15 texture, precipitation pulses, and antecedent conditions on the relative importance of NSS soil
16 CO₂ behavior, and to identify the factors giving rise to such behavior. We simulated soil CO₂
17 concentrations, CO₂ production, and R_{soil} under four different soil textures and three different
18 precipitation regimes. For each scenario, we implemented the DETECT model under the
19 assumption that soil CO₂ production is affected by antecedent moisture and temperature versus
20 the assumption that only concurrent conditions matter. Data from the Wyoming Prairie Heating
21 and CO₂ Enrichment (PHACE) experiment (e.g., Carrillo et al., 2014a; Mueller et al., 2016;
22 Pendall et al., 2013; Ryan et al., 2015; Zelikova et al., 2015) were used to parameterize the
23 model and motivated the selection of the texture and precipitation scenarios. Under the different



1 scenarios, we compared R_{soil} and CO_2 production rates predicted from the DETECT model to
2 that of a simpler SS model, and evaluated the relative impact of SS assumptions on inferring
3 subsurface processes (e.g., CO_2 production by roots and microbes) and surface CO_2 fluxes (i.e.,
4 R_{soil}).

5 **2. Methods**

6 Our DETECT model simulates CO_2 production by roots and microbes at 100 0.01-m depth
7 intervals at 6-hourly time increments, but it is flexible enough to accommodate finer or coarser
8 depth and time intervals. The backbone of DETECT is a partial differential equation (PDE)
9 model motivated by diffusion theory, and solved numerically. In this study, we used the
10 DETECT model to simulate time- and depth-varying soil CO_2 concentration and CO_2 production
11 rates and time-varying surface soil CO_2 efflux (R_{soil}) over 183 days demarking the growing
12 season in a mixed-grass prairie in south-central Wyoming. The model is driven by environmental
13 data collected at the Prairie Heating and CO_2 Enrichment (PHACE) experiment near Cheyenne,
14 Wyoming (Pendall et al., 2013). PHACE data were also used to derive realistic parameter values
15 associated with the submodels for CO_2 production and diffusivity, and additional data were used
16 to qualitatively evaluate model predictions.

17 In this section, we describe key components of the DETECT model (section 2.1), the
18 numerical solution approach (section 2.2), and the SS solution to the underlying PDE (section
19 2.3). We follow this by a description of how we parameterized the model to be representative of
20 a “real” system by drawing upon information from the PHACE experiment (section 2.4). This
21 leads us to provide an overview of the PHACE experiment and relevant datasets used to
22 parameterize, drive, and informally test the model. We conclude this methods section by
23 outlining the simulation experiments that we conducted with the DETECT model and its SS



1 counterpart to evaluate the influence of soil texture and precipitation variability on SS versus
2 NSS soil CO₂ behavior (section 2.5).

3 **2.1 Description of the Non Steady State DETECT Model**

4 The PDE that underlies the DETECT model (v1.0) accounts for time- and depth-varying CO₂
5 diffusivity and CO₂ production by root and microbial respiration (Fang & Moncrieff, 1999). We
6 use a pair of PDEs, one describing the soil CO₂ derived from root respiration (subscripted with
7 R), and the other for CO₂ derived from microbial respiration (M) such that for $K = R$ or M :

$$\frac{\partial c_K(z,t)}{\partial t} = \frac{\partial}{\partial z} \left(D_{gs}(z,t) \frac{\partial c_K(z,t)}{\partial z} \right) + S_K(z,t) \quad (1)$$

8 $c_K(z,t)$ is CO₂ concentration (mg CO₂ m⁻³), $D_{gs}(z,t)$ is the effective diffusivity of CO₂ through the
9 soil (m² s⁻¹), and $S_K(z,t)$ is the source (or production) term (mg CO₂ m⁻³) (Fig. 1b), all of which
10 vary by depth z (meters) and time t (hours). Note that D_{gs} is assumed to be the same for root- and
11 microbial-derived CO₂ and is thus not indexed by K . In this version of the model, we assumed
12 that CO₂ transport within the soil profile and over time is solely governed by gaseous diffusion,
13 and we ignored other types of CO₂ transport—such as diffusion in the liquid state, convection,
14 and bulk transport via vertical movement of water—that have been shown to have a negligible
15 contribution (Fang and Moncrieff, 1999; Kayler et al., 2010). Total soil CO₂ and total CO₂
16 production are given as $c(z,t) = c_M(z,t) + c_R(z,t)$ and $S(z,t) = S_M(z,t) + S_R(z,t)$, respectively. Below
17 we describe the two main components of the PDE model: (1) CO₂ diffusivity, D_{gs} , and (2) the
18 production terms, $S_R(z,t)$ and $S_M(z,t)$.

19 *2.1.1 Soil CO₂ diffusivity sub-model*

20 The diffusivity of CO₂ within the soil (D_{gs}) depends on soil structure and water content; we



1 modeled D_{gs} using the Moldrup function (Moldrup et al., 2004; Sala et al., 1992). We chose this
 2 formulation because it is more accurate than other common models, such as the Millington and
 3 Quirk (2000) and Penman (1981) models (Moldrup et al., 2004). Based on Moldrup et al. (2004),
 4 D_{gs} ($\text{m}^2 \text{s}^{-1}$) is defined as:

$$5 \quad D_{gs}(z, t) = D_{g0}(z, t) \cdot (2\phi_{g100}(z)^3 + 0.04\phi_{g100}(z)) \cdot \left(\frac{\phi_g(z, t)}{\phi_{g100}(z)} \right)^{2 + \frac{3}{b(z)}}, \quad (2)$$

6 where $D_{g0}(z, t) = D_{stp} \cdot \left(\frac{T_s(z, t)}{T_0} \right)^{1.75} \cdot \left(\frac{P_0}{P(t)} \right)$ and $D_{stp} = 1.39 \times 10^{-5} \text{ m}^2 \text{ s}^{-1}$ is the diffusion
 7 coefficient for CO_2 in air at standard temperature (T_0 , 273 K) and pressure (P_0 , 101.325 kPa);
 8 $T_s(z, t)$ is the soil temperature (Kelvin) at depth z and time t , and $P(t)$ is the air pressure (kPa) just
 9 above the soil surface at time t . The remaining terms in Eqn 2 include $\phi_g(z, t)$, the air-filled soil
 10 porosity, which is related to the total soil porosity (ϕ_T) and volumetric soil water content (θ)
 11 according to $\phi_g(z, t) = \phi_T(z) - \theta(z, t)$, and $\phi_T(z)$ is defined as $1 - \text{BD}(z)/\text{PD}$, where BD and PD are
 12 the bulk density and particle density of the soil, respectively; $\phi_{g100}(z)$ is the air-filled porosity at a
 13 soil water potential (Ψ) of -100 cm H_2O (about -10 kPa); $b(z)$ is a unitless parameter that is
 14 related to the pore size distribution of the soil based on the water retention curve given by $\Psi =$
 15 $\Psi_e(\theta/\theta_{sat})^{-b}$, where $\Psi_e(z)$ is the air-entry potential and $\theta_{sat}(z)$ is the saturated soil water content
 16 (v/v).

17 2.1.2 CO_2 source (production) terms

18 Soil CO_2 can be produced in the soil (S term in Eqn. 1) by five different biological processes: (i)
 19 root growth respiration, (ii) root maintenance respiration, (iii) consumption of rhizodeposits by
 20 root-associated microorganisms and associated microbial respiration, (iv) microbial



1 decomposition of newly produced plant litter that has been incorporated into the soil matrix, and
 2 (v) microbial decomposition of older soil organic matter (SOM) (Pendall et al., 2004). Due to the
 3 general lack of sufficient data and process understanding to accurately separate all five sources,
 4 the DETECT model treats CO₂ production as the sum of two main contributions: CO₂ respired
 5 by (1) roots and closely associated microorganisms (the sum of (i)-(iii)), giving $S_R(z,t)$, and (2)
 6 free-living soil microorganisms (the sum of (iv)-(v)), giving $S_M(z,t)$. Such simplification based on
 7 root and microbial sources is common in models of soil CO₂ transport and production (Fang and
 8 Moncrieff, 1999; Hui and Luo, 2004; Šimůnek and Suarez, 1993). Although DETECT v1.0
 9 assumes that root and microbial respiration are independent of one another, they both depend on
 10 the same environmental data (e.g., θ and T_s).

11 CO₂ production by root respiration is represented as the product of three terms: (i) the
 12 mass-specific base respiration rate (R_{Rbase}) at a reference soil temperature of $T_s = T_{ref}$, and at
 13 average soil water and antecedent temperature conditions, (ii) root mass expressed as the amount
 14 of root carbon, $C_R(z,t)$, and (iii) functions that rescale R_{Rbase} to account for the effect of soil water
 15 (θ), temperature (T_s), and their antecedent counterparts, which are determined separately for
 16 roots and microbes. For roots, antecedent soil water and temperature are denoted as θ_R^{ant} and
 17 T_s^{ant} , respectively. In general, $S_R(z,t)$ is given by:

$$S_R(z,t) = R_{Rbase} \cdot C_R(z,t) \cdot f(\theta(z,t), \theta_R^{ant}(z,t)) \cdot g(T_s(z,t), T_s^{ant}(z,t)) \quad (3)$$

18 The functional form of $C_R(z,t)$ is informed by field data on root biomass C (see Appendix S1 for
 19 complete details). The functions f and g are given by:

$$f(\theta, \theta_R^{ant}) = \exp(\alpha_1 \theta(z,t) + \alpha_2 \theta_R^{ant}(z,t) + \alpha_3 \theta(z,t) \cdot \theta_R^{ant}(z,t)) \quad (4a)$$

$$g(T_s, T_s^{ant}) = \exp\left(E_o(z,t) \cdot \left(\frac{1}{T_{ref} - T_o} - \frac{1}{T_s(z,t) - T_o}\right)\right) \quad (4b)$$



$$E_o(z, t) = E_o^* + \alpha_4 T_s^{ant}(z, t) \quad (4c)$$

1 $\alpha_1, \alpha_2, \alpha_3, \alpha_4, T_o$, and E_o^* are parameters that require numerical values (Table 1; Ryan et al.
 2 2015), θ and T_s are informed by field data, and θ_R^{ant} and T_s^{ant} are computed from the field data
 3 (described below). The temperature scaling function, g (Eqn 4b), is motivated by Lloyd and
 4 Taylor (1994) and has been successfully used to describe soil and ecosystem respiration (Cable
 5 et al., 2013; Luo and Zhou, 2010; Ryan et al., 2015). $E_o(z, t)$ is analogous to an energy of
 6 activation term that governs the apparent temperature sensitivity of S_R (Cable et al., 2011;
 7 Davidson and Janssens, 2006; Tucker et al., 2013); we assume E_o responds to antecedent
 8 temperature, reflecting a potential thermal acclimation response (Atkin and Tjoelker, 2003; Ryan
 9 et al., 2015). T_o is also related to the apparent temperature sensitivity (Cable et al., 2011), and
 10 we assume that it is invariant with depth and time (Barron-Gafford et al., 2014; Cable et al.,
 11 2013; Lloyd and Taylor, 1994; Ryan et al., 2015). An exponential function is also used for the
 12 moisture scalar, f , to ensure $f > 0$ (Eqn 4a). While the functional forms and choice of
 13 environmental drivers used for f and g were motivated by previous analyses (Barron-Gafford et
 14 al., 2014; Cable et al., 2013), the exact functions and parameter values were based on Ryan et al.
 15 (2015) and Cable et al. (2013).

16 CO_2 production by microbial respiration and SOM decomposition is represented by a
 17 modified version of the Dual Arrhenius and Michaelis-Menten (DAMM) model (Davidson et al.,
 18 2012). We exclude the O_2 term, rendering the model relevant to systems that are typically
 19 unlimited by O_2 availability, such as the semi-arid site that we focus on, but we accounted for a
 20 microbial C pool (C_{MIC}) and a soluble soil-C pool (C_{SOL}) (Todd-Brown et al., 2012) such that:

$$S_M(z, t) = V_{max}(z, t) \cdot \frac{C_{SOL}(z, t)}{K_m + C_{SOL}(z, t)} \cdot C_{MIC}(z, t) \cdot (1 - CUE) \quad (5)$$



1 Decomposition is assumed to be an enzymatic process that follows Michaelis-Menten kinetics,
 2 where V_{max} is the maximum potential decomposition rate, and K_m (the half-saturation constant) is
 3 the amount of substrate required for the decomposition rate to reach half of V_{max} . Carbon-use
 4 efficiency (CUE) represents the proportion of total C assimilated by microbes that is allocated
 5 for microbial growth (Tucker et al., 2013). We excluded a microbial death rate term (Todd-
 6 Brown *et al.*, 2012) because we had insufficient data on death rates, and C_{MIC} is only ~1% of
 7 C_{SOL} at our study site (Carrillo and Pendall, in review).

8 In contrast to the original DAMM formulation, we allowed $S_M(z,t)$ and $V_{max}(z,t)$ to vary
 9 by depth and time, whereas existing applications of the DAMM model are generally applied to
 10 “bulk” soil (i.e., do not vary with z). We also modeled V_{max} according to the modified energy of
 11 activation function described in Lloyd and Taylor (1994), which essentially parallels Eqns 4b-4c:

$$12 \quad V_{max}(z,t) = V_{Base} \cdot f(\theta, \theta_M^{ant}) \cdot \exp\left(E_o(z,t) \cdot \left(\frac{1}{T_{ref} - T_o} - \frac{1}{T_S(z,t) - T_o}\right)\right) \quad (6)$$

13 V_{Base} is the ‘base’ V_{max} at a reference soil temperature of T_{ref} and at mean values of current θ and
 14 antecedent θ and T_S (i.e., mean values of θ_M^{ant} and T_S^{ant}). $E_o(z,t)$ and $f(\theta, \theta_M^{ant})$ follow the same
 15 functional forms and interpretation as described for the root respiration submodel (Eqns 3 and
 16 4a-c), except that θ_M^{ant} and T_M^{ant} are used instead of θ_R^{ant} and T_R^{ant} , respectively, and different
 17 values are specified for the parameters $\alpha_1, \alpha_2, \alpha_3, \alpha_4, T_o$, and E_o^* to reflect microbial respiration
 18 (see Table 1).

19 Finally, C_{SOL} is modeled as a function of soil organic C content at depth z , $C_{SOM}(z)$, based
 20 on the fraction, p , of $C_{SOM}(z)$ that is soluble and the diffusivity of the substrate in liquid, D_{liq}
 21 (Davidson et al., 2012). The equation for C_{SOL} is given by:

$$C_{SOL}(z,t) = C_{SOM}(z) \cdot p \cdot \theta(z,t)^3 \cdot D_{liq} \quad (7)$$



1 The values of p and D_{liq} were taken from laboratory analysis (see § 2.4.5) and Davidson et al.
 2 (2012), respectively. We assumed that $C_{SOM}(z)$ and $C_{MIC}(z)$ (see Eqn 5) are constant over time
 3 given the relatively short simulation periods we explored here (a single growing season); but the
 4 model could be easily modified to allow for time-vary C_{SOM} and C_{MIC} . Here, $C_{SOM}(z)$ and $C_{MIC}(z)$
 5 are simple, empirical functions that were informed by data (see Appendix S1 for details).
 6 Moreover, while assumption of time invariant $C_{SOM}(z)$ and $C_{MIC}(z)$ is an implicit SS assumption
 7 about biological factors affecting soil CO₂ dynamics, this assumption allows us to isolate the
 8 importance of NSS conditions that are primarily due to physical CO₂ transport characteristics.

9 2.1.3 Soil respiration

10 The efflux of CO₂ from the soil surface (soil respiration, R_{soil}) is computed as:

$$11 \quad R_{soil}(t) = \frac{D_{gs}(z=0.01, t)}{\Delta z} (c(z=0.01, t) - c_{atm}(t)) \quad (8)$$

12 $D_{gs}(z=0.01, t)$ is the diffusivity of CO₂ in the soil and $c(z=0.01, t)$ is the total CO₂ concentration
 13 (microbial- and root-derived), respectively, at $z = 0.01$ m depth and time t ; $c_{atm}(t)$ is the CO₂
 14 concentration in the atmosphere above the soil surface; and Δz is the depth increment that the
 15 model solves for soil CO₂ concentration (here, $\Delta z = 0.01$ m).

16 2.2 Numerical implementation of the DETECT model

17 The numerical solution to the NSS version of the DETECT model v1.0, as described in Eqns 1-8,
 18 requires an initial condition (IC) and two boundary conditions (BCs), which we specified as:

$$19 \quad \text{IC:} \quad c(z, t = 0) = c_0(z) \quad (9a)$$

$$20 \quad \text{Upper BC:} \quad c(z = 0, t) = c_{atm}(t) \quad (9b)$$

$$21 \quad \text{Lower BC:} \quad \frac{\partial c(z = 1, t)}{\partial z} = 0 \quad (9c)$$



1 The function $c_0(z)$ is determined and parameterized using observed soil CO₂ concentration data
 2 at three depths (Appendix S2, supplemental material); we set $c_{atm}(t)$ equivalent to 356 ppm for all
 3 t , which was the average near-surface, ambient atmospheric CO₂ concentration measured at the
 4 PHACE site in the 2008 growing season. Following methods of Haberman (2015), we adopted a
 5 zero-flux lower BC (Eqn 9c) due to the lack of data at or near a depth of 1 m.

6 We numerically solved the non-linear PDE (Eqn. 1) by employing a forward Euler
 7 discretization with a centered difference method for the depth derivative at a depth increment of
 8 $\Delta z = 0.01$ m. To ensure numerical stability, we calculate model outputs at a numerical time-step
 9 of $\Delta t = \frac{dt}{Ndt}$, where dt is the time step at which the predicted outputs are stored (6 hours), and
 10 Ndt is the number of numerical time-steps. Ndt is computed based on the fastest (largest)
 11 diffusion coefficient at each time step such that $Ndt \geq \frac{dt \times \max(D_{gs})}{0.5 \times (\Delta z)^2}$, where $\max(D_{gs})$ is the
 12 maximum D_{gs} across all depth increments at time t (Haberman, 1998). We solved Eqn. 1
 13 separately for both root- and microbial-derived CO₂ concentrations, such that for $K = R$ or M :

$$\begin{aligned}
 14 \quad \frac{c_K(z, t + \Delta t) - c_K(z, t)}{\Delta t} &= D_{gs}(z, t) \left(\frac{c_K(z + \Delta z, t) - 2c_K(z, t) + c_K(z - \Delta z, t)}{(\Delta t)^2} \right) \\
 15 \quad &+ \left(\frac{D_{gs}(z + \Delta z, t) - D_{gs}(z - \Delta z, t)}{2\Delta z} \right) \left(\frac{c_K(z - \Delta z, t) - c_K(z + \Delta z, t)}{2\Delta z} \right) \\
 16 \quad &+ S_K(z, t) \tag{10}
 \end{aligned}$$

17 We rearranged Eqn. 10 to solve for $c_K(z, t + \Delta t)$, which was iterated forward for all time-steps and
 18 depth increments; total CO₂ concentration at each time step and depth is calculated as $c(z, t + \Delta t) =$
 19 $c_R(z, t + \Delta t) + c_M(z, t + \Delta t)$. We programmed the DETECT model v.10 and the numerical solution
 20 method in Matlab (Mathworks, 2016).

21



1 **2.3 Steady-state (SS) solution to the DETECT model**

2 A primary goal of this work was to test if soil CO₂ and associated R_{soil} predicted from the non-
 3 steady-state (NSS) model (DETECT) could be distinguished from that of the steady-state (SS)
 4 solution. The SS version of Eqn 1, which we refer to as the SS-DETECT model, can be solved
 5 analytically as an ordinary differential equation (ODE) by setting the $\partial c/\partial z$ term to zero
 6 (Amundson et al., 1998). As with the NSS model, we found the SS solution to Eqn. 1 separately
 7 for root- and microbial-derived CO₂ concentrations, $c_R^*(z,t)$ and $c_M^*(z,t)$, respectively. Using the
 8 upper and lower boundary conditions described for the NSS model (Eqns 9b and 9c), the
 9 analytical SS solutions at time t and depth z are derived by Amundson et al. (1998) and given by,
 10 for $K = R$ and M :

$$11 \quad c_K^*(z,t) = \frac{S_K^*(t)}{D_{gs}(z,t)} \left(z - \frac{z^2}{2} \right) + c_{atm}(t) \quad (11a)$$

$$12 \quad S_K^*(t) = \frac{1}{100} \sum_{z=0.01}^{1m} S_K(z,t) \quad (11b)$$

13 $S_K^*(t)$ is the depth-averaged source term for microbial or root production (averaging over 100
 14 0.01-m increments). The soil CO₂ diffusivity term, $D_{gs}(z,t)$, and upper boundary condition,
 15 $c_{atm}(t)$, are the same as previously defined (Eqns 2 and 9b, respectively; Amundson *et al.* (1998)).

16 **2.4 Application of the DETECT and SS-DETECT models to the PHACE site**

17 To address our research questions related to the relative importance of NSS versus SS conditions
 18 for understanding and modeling soil CO₂ transport and fluxes (e.g., R_{soil}), we applied the
 19 DETECT and SS-DETECT models to data obtained from a semi-arid grassland in Wyoming. We
 20 expected that the precipitation pulse regimes characteristic of this and other semi-arid
 21 ecosystems would likely lead to NSS soil CO₂ conditions given the impacts of such pulse



1 regimes on soil water dynamics (Bachman et al., 2010; Kemp et al., 1997; Reynolds et al., 2004;
2 Sala et al., 1992; Sala et al., 1981). For example, pulse-driven, semi-arid ecosystems can
3 experience long periods of dry soil conditions, under which SS soil CO₂ conditions likely
4 operate, interrupted by moisture pulses that we would expect to cause transient NSS conditions
5 due to rapid changes in soil air-filled porosity, temperature, and associated soil CO₂ diffusivity.
6 These NSS conditions would also likely be associated with high flux rates (e.g., high CO₂
7 production rates and high R_{soil}), potentially making such transient conditions proportionally
8 more important over the long-term (Jarvis et al., 2007).

9 Thus, in this subsection, we provide an overview of the study site, including the PHACE
10 experiment, and relevant data sources from PHACE that we used to drive the DETECT and SS-
11 DETECT models. We also summarize how we calibrated the models in the context of the
12 PHACE site, and we highlight data that we used to informally validate the general behavior of
13 the models. We conclude by describing the simulation experiments that we conducted to test the
14 effects of soil texture and precipitation variability on the importance of NSS versus SS soil CO₂
15 conditions.

16 *2.4.1 Field site and PHACE experiment*

17 The Prairie Heating and CO₂ Enrichment (PHACE) field experiment is located in south-central
18 Wyoming (latitude 41° 50'N, longitude 104° 42'W, elevation = 1930 m). The site is a mixed-
19 grass prairie with a semi-arid climate characterized by long winters (mean January temperature =
20 -2.5 °C) and warm summers (mean July temperature = 17.5 °C), with mean annual precipitation
21 of 384 mm (Morgan et al., 2011). The vegetation is predominantly composed of two C₃ grasses,
22 western wheatgrass (*Pascopyrum smithii* (Rydb.) A. Löve) and needle-and-thread grass
23 (*Hesperostipa comata* Trin and Rupr), and a C₄ perennial grass, blue grama (*Bouteloua gracilis*



1 (H.B.K.) Lag). The soil is a fine-loamy, mixed, mesic Aridic Argiustoll, and biological crusts are
2 not present (Bachman et al., 2010).

3 2.4.2 Environmental driving data

4 We simulated the transport and production of soil CO₂ for each 0.01 m depth increment, from the
5 surface (0 m) to 1 m, across all 732 time steps (i.e., 4 time steps per day [every 6 hours] for 183
6 days from April-September). To do this, we required soil environmental data consisting of water
7 content (θ) and temperature (T_S) and meteorological data including precipitation, air temperature,
8 and air pressure. The PHACE study provided these data, or data that were used to create the
9 driving data at the necessary spatial and temporal resolution.

10 The PHACE experiment involved an incomplete factorial of CO₂, warming, and
11 irrigation (6 treatment levels total), with five replicate plots per treatment level, resulting in a
12 total of 30 instrumented plots. One of the five plots from the control treatment—ambient CO₂,
13 temperature (no heating), and precipitation (no supplemental irrigation)—was chosen at random
14 and had a system installed to measure soil CO₂ concentrations continuously for three different
15 soil depths (3, 10, and 20 cm). This plot, therefore, provided the data for driving the DETECT
16 and SS-DETECT models. Data that we used were collected during the growing season (March-
17 September) of 2008; θ was measured hourly at three depths (5-15, 15-25, and 35-45 cm;
18 EnvironSMART probe, Sentek Sensor Technologies, Stepney, Australia), and we used daily
19 averages to drive the models. T_S was measured hourly at two depths (3 and 10 cm) using type-T
20 thermocouples. Likewise, hourly precipitation (mm), air temperature (°C), relative humidity (%),
21 and surface barometric air pressure (kPa) were recorded by an automated weather station at the
22 site.



1 2.4.3 High resolution environmental data

2 To accommodate the 0.01 m depth increments specified for the DETECT model, we used the
3 coarse resolution field data (above) to create finer resolution driving data. For example, temporal
4 gap-filling of the θ , T_S , and micrometeorological datasets was required due to gaps that occurred
5 during a small number of days (<1%, 6%, and 2.5%, respectively) as a result of instrument
6 failure. We used data from other nearby plots to estimate the values of the missing data, but we
7 also used cubic spline interpolation where gaps remained. Details of these gap-filing methods
8 can be found in Ryan *et al.* (2015).

9 We used HYDRUS-1D v4.16.0090 to simulate θ and T_S in 0.01 m increments from a
10 depth of 0.01 m to 1 m (Chou *et al.*, 2008; Piao *et al.*, 2009; Šimůnek *et al.*, 2008) based on
11 precipitation data at the site. HYDRUS simulates the movement of water by solving the
12 Richards' equation for water movement (Chou *et al.*, 2008; Richards, 1931; Sitch *et al.*, 2008)
13 and heat transport via Fickian based advection-dispersion equations. Soil hydraulic and heat
14 transport parameters were estimated in HYDRUS using the inverse mode to solve for parameter
15 values based on the PHACE θ (5-10, 15-25, and 35-45 cm) and T_S (3 and 10 cm) data.
16 HYDRUS was then run in forward mode based on the tuned soil hydraulic parameters to
17 estimate θ and T_S at all 100 0.01-m depth increments at 6-hourly time intervals. For consistency,
18 HYDRUS-derived θ and T_S were used as the environmental input data to the DETECT models,
19 even at the depths for which PHACE data were available.

20 2.4.4 Antecedent soil water and soil temperature conditions

21 We explicitly evaluated the impact of antecedent (past) θ and T_S conditions on CO₂ production
22 by roots and microbes, motivated by prior work that estimated the relative importance of
23 antecedent conditions and their time-scales of influence on soil and ecosystem CO₂ efflux



1 (Barron-Gafford et al., 2014; Cable et al., 2013; Ogle et al., 2015; Ryan et al., 2015). Antecedent
 2 soil water content and antecedent soil temperature— $\theta_R^{ant}(z,t)$ and $T_s^{ant}(z,t)$, respectively, for $K =$
 3 R (roots) and M (microbes)—were computed as weighted averages of the HYDRUS-produced
 4 $\theta(z,t)$ and $T_s(z,t)$ data, respectively. These calculations were done external to the DETECT
 5 model, and the antecedent variables were supplied as driving variables to DETECT. For
 6 example, for each 0.01 m increment (z) and time period (t), antecedent soil water associated with
 7 microbial CO₂ production was calculated as:

$$8 \quad \theta_M^{ant}(z,t) = \sum_{j=1}^J w(j) \cdot \theta(z,t-j) \quad (12)$$

9 The w 's are the antecedent importance weights, which sum to 1 from $j = 1$ (previous time period)
 10 to $j=J$ (J time periods previous). The weights were informed by results from an analysis of
 11 ecosystem respiration at the PHACE site (Ryan et al., 2015). For microbes, $J = 4$ days and $w =$
 12 $(0.75, 0.25, 0, 0)$, indicating the strong importance of θ conditions occurring yesterday ($j = 1$)
 13 (Oikawa et al., 2014). Similar equations were used to compute $\theta_R^{ant}(z,t)$ and $T_s^{ant}(z,t)$, each with
 14 their own set of weights (w 's) and time-scales (J 's). For example, the time step and J for θ differ
 15 among microbes (2 days) and roots (3 weeks); for roots, $\theta_R^{ant}(z,t)$ was computed as a weighted
 16 average of past, average weekly values of θ , with j denoting weeks into the past, for $J = 4$ weeks,
 17 and $w = (0.2, 0.6, 0.2, 0)$, indicating a strong lag response to θ conditions occurring two weeks
 18 ago (Cable et al., 2013; Ryan et al., 2015). For antecedent soil temperature, we assumed that
 19 each of the past four days were equally important by setting the w vectors to $(0.25, 0.25, 0.25,$
 20 $0.25)$, for both microbes and roots (Ryan et al., 2015). The specification of J and the w 's are
 21 independent of the DETECT model formulation and can be varied by the user. Specifically, the
 22 antecedent drivers become input variables that are specified outside of the DETECT machinery.



1 2.4.5 Overview of parameterization approach using PHACE data

2 In general, our aim was to specify realistic values for the parameters in the DETECT model. We
3 did not formally “fit” the DETECT model to data, but rather, we simply determined reasonable
4 values based on simple analyses of relevant PHACE data sets, results published for the PHACE
5 site, or results from other relevant studies. For clarity, we categorize the parameters into four
6 groups (Table 1). The first group consists of parameters used solely for the microbial source or
7 production term (S_M , Eqns 5-6), and the second group of parameters belong solely to the root
8 respiration source term (S_R , Eqns 3-4). Parameters in the third group are shared between the S_M
9 and S_R submodels; the fourth group contains parameters associated with calculating CO₂
10 diffusivity (D_{gs} , Eqn 2). The full list of parameters is given in Table 1, and below we describe the
11 logic behind specifying specific values in Table 1.

12 The depth-distributions of root biomass C (C_R , Eqn 3), soil microbial biomass C (C_{MIC} ,
13 Eqn 5), and soil organic C (C_{SOM} , Eqn 7) are expressed in terms of a total C content in a 1 m
14 deep soil column (e.g., R^* , M^* , and S^* , respectively; mg C cm⁻²), multiplied by the proportion of
15 that C that occurs at depth z (e.g., f_R , f_M , and f_S , respectively). For example, $C_R(z,t) =$
16 $R^* \cdot f_R(z) \cdot G(t)$, where $G(t)$ is a function that scales R^* by an index of time-varying vegetation
17 activity based on vegetation greenness estimates (Pendall et al., 2001; Appendix S1). The depth-
18 varying distributions of C contents were approximated by fitting a simple exponential function to
19 data on root, microbial, and soil organic C content, thus providing estimates for R^* , M^* , S^* , $f_R(z)$,
20 $f_M(z)$, and $f_S(z)$ (see Appendix S1 for details; Table 1). Regarding the data, soil organic C was
21 determined by combustion of acidified, root-free soil collected from 0-5, 5-15, 15-30, 30-45, 45-
22 75, and 75-100 cm depths, using a Costech Elemental Analyzer. Microbial biomass C was
23 determined by the chloroform fumigation and extraction in 0.05 M K₂SO₄ (Carrillo et al.,



1 2014b). Extracts were analysed for total C on a total organic carbon analyzer (Shimadzu TOC-
2 VCPN; Shimadzu Scientific Instruments, Wood Dale, IL, USA) after treating with 1 M H₃PO₄
3 (1 µl per 10 ml of extract) to remove any carbonates. Root biomass C was estimated from ash-
4 free root biomass and elemental analysis (Carrillo et al., 2014a; Mueller et al., 2016). The
5 solubility parameter, p , was estimated as the ratio of C_{SOL} to C_{SOM} (Eqn 7), and was based on
6 unfumigated extracts obtained for microbial biomass estimations as above (C_{SOL}) and on total C
7 concentration in soil (C_{SOM}).

8 The values used for the base microbial respiration rates and the half-saturation constant
9 (V_{Base} [Eqn 6] and K_m [Eqn 5]; Table 1) were estimated by fitting the microbial respiration
10 submodel, but without the C_{MIC} or CUE terms (Eqn 5), to microbial respiration data from the
11 PHACE control plots (Fig. S6). In the absence of root respiration data, we assumed that base
12 root respiration (R_{Rbase} [Eqn 3]; Table 1) was proportional to the microbial base rate term
13 (Hanson et al., 2000). The parameters denoting the effects of current soil moisture (e.g., α_1 ; Eqn
14 4a), antecedent moisture (α_2), and the interaction between current and antecedent moisture (α_3)
15 on root and microbial respiration were derived from Ryan *et al.* (2015), also based on an analysis
16 of ecosystem respiration (R_{eco}) data from PHACE. However, we adjusted the values (Table 1) to
17 reflect the expectation that the effects of current soil moisture should be stronger for microbial
18 compared to root respiration because microbes tend to respond more rapidly to precipitation
19 pulses (Risk et al., 2008), whereas root respiration is likely to show a delayed response that
20 depends more strongly on past moisture conditions (Cable et al., 2013; Cable et al., 2008). Of
21 the remaining two parameters describing S_M (Eqns 5-6; Table 1), the value of CUE was based on
22 results from a soil incubation study conducted at a nearby site (Tucker et al., 2013), whilst our
23 value for D_{liq} was taken from Davidson *et al.* (2012). Three parameters (E_o^* , T_o , and α_4 ; Eqns



1 4a-b) were shared between the S_R and S_M submodels, and their values were also obtained from
2 Ryan *et al.* (2015). Finally, the parameters used for CO₂ diffusivity (b , BD , and ϕ_{g100} ; Eqn 2)
3 were based on published, site-specific data (Morgan *et al.*, 2011).

4 2.4.6 Informal model validation with soil respiration measurements

5 We evaluated the accuracy of the DETECT model by comparing (1) predicted R_{soil} (Eqn 8)
6 against plot-level measurements of ecosystem respiration (R_{eco}) (see below) and (2) predicted
7 soil CO₂ concentrations, $c(z,t)$, versus observed concentrations; all observed data were from the
8 PHACE study. Since we did not rigorously parameterize the DETECT model with PHACE data,
9 we were simply looking for reasonable, qualitative agreement between the modelled variables
10 and the observations (e.g., similar order of magnitude, comparable temporal trends). Observed
11 R_{eco} was measured on control plots every 2–4 weeks during the target growing season, using a
12 canopy gas exchange chamber, and instantaneous fluxes were scaled to daily rates using a linear,
13 empirical function (Bachman *et al.*, 2010; Jasoni *et al.*, 2005). We assumed that R_{soil} was similar
14 to R_{eco} given that aboveground biomass was <20% of total plant biomass (Mueller *et al.*, 2016).
15 Glyphosate herbicide was applied to small subplots in May, 2008, limiting ecosystem CO₂ efflux
16 to microbial sources (Pendall *et al.*, 2013), and non-steady state soil chambers were used to
17 estimate surface soil fluxes every two weeks around midday (Ogle *et al.*, 2016; Oleson *et al.*,
18 2013); these data provided observations of microbial respiration. Soil CO₂ concentrations were
19 also measured with non-dispersive infrared sensors (Vaisala GM222, Finland) installed at 3, 10,
20 and 20 cm below the soil surface, averaged on an hourly basis (Brennan, 2013; Risk *et al.*, 2008;
21 Vargas *et al.*, 2011). Observations of soil [CO₂] for control plots were compared against
22 predictions of $c(z,t)$ at $z = 0.03, 0.1, \text{ and } 0.2$ m and at the corresponding times.

23



1 2.5 Simulation Experiments

2 We evaluated the impact of three potentially important factors that could affect the frequency of
3 NSS (Eqns 1 and 9a-c) relative to SS (Eqn 10) conditions: (1) soil texture, (2) precipitation
4 patterns, and (3) importance of antecedent conditions. In the control (*Ctrl*) scenario, we
5 calculated the source terms and diffusion terms (S_K and D_{gs} in Eqns 1 and 2) based on soil
6 environmental (θ and T_S), soil texture (sandy clay loam: 60% sand, 20% silt, 20% clay), and
7 meteorological data (e.g., precipitation) measured at the PHACE site in 2008. We varied soil
8 texture, relative to that of the site, by varying the relative amounts of sand, silt, and clay, giving
9 three levels (Table 3): 80% sand, 10% silt, and 10% clay (sandy loam, scenario denoted as *ST-*
10 *Sa*); 20% sand, 60% silt, and 20% clay (silt loam, *ST-Si*); 20% sand, 20% silt, and 60% clay
11 (clay, *ST-Cl*). The control (*Ctrl*) scenario was also paired with the observed daily precipitation
12 data for 2008. We explored three additional precipitation scenarios, under the control soil
13 texture, by shifting the daily precipitation to occur one month earlier, or one month later, or by
14 using precipitation data from 2009 (scenarios *P-E*, *P-L* and *P-FM*, respectively; Table 3). For *P-*
15 *FM*, we chose 2009 because it had approximately the same total precipitation between April and
16 September as 2008, but it fell as more frequent events of smaller magnitudes. For each texture
17 and precipitation scenario, HYDRUS was used to compute the corresponding T_S and θ at the
18 required depth and time intervals. All above scenarios assumed that antecedent conditions are not
19 important, which was achieved by setting all antecedent effects parameters (α_2 , α_3 , and α_4 ; Table
20 1) equal to zero. We contrasted these scenarios against ones that included antecedent conditions
21 (thus, computed θ_K^{ant} and T_S^{ant} in Eqs 3 and 6) in the calculation of soil CO₂ production by roots
22 ($K=R$) and microbes ($K=M$); all such scenario names were appended with “*ant*” (Table 3, Fig.



1 1a). For each scenario summarized in Table 3, we evaluated the potential for NSS conditions by
2 comparing the predicted R_{soil} produced by the DETECT model versus the SS-DETECT model.

3 **3. Results**

4 Our analysis indicated that soil texture was the strongest predictor of whether soil CO₂ and
5 associated R_{soil} were in steady state or not, particularly during periods of high precipitation. Thus,
6 precipitation patterns played a secondary role. The inclusion of antecedent soil water and soil
7 temperature effects in the model resulted in a significant increase in predicted annual R_{soil} but
8 only for the control and fine textured soil scenarios, and resulted in predicted soil CO₂ being
9 closer to soil CO₂ measurements from the PHACE site. Below, we summarize key results from
10 this study.

11 **3.1 Control Scenarios**

12 Soil CO₂ was in steady state (SS) during most of the growing season under the control soil
13 texture (sandy clay loam) and precipitation conditions that assumed no antecedent affects (*Ctrl*
14 scenario). For example, soil respiration (R_{soil}) predicted by the DETECT model was
15 approximately equal to R_{soil} predicted by the SS-DETECT model during times of no or little
16 precipitation (Fig. 2a, days < 218 or > 230). Conversely, R_{soil} predicted by the SS-DETECT
17 model was temporarily greater and more variable than that predicted by the DETECT model
18 immediately following a large precipitation event (Fig. 2a, days 218-229). However, the total
19 cumulative R_{soil} between days 92 to 274 – hereafter ‘total growing season R_{soil} ’ – under SS (497
20 g C m⁻²) versus NSS (498 g C m⁻²) assumptions was approximately equal (a difference of
21 ~0.2%).



1 The effects of antecedent conditions (*Ctrl-ant* scenario; Fig. 2b) were generally consistent
2 with the control scenario without antecedent conditions. However, the magnitude of R_{soil}
3 predicted by both the DETECT and SS-DETECT models was up to $9 \text{ gC m}^{-2} \text{ day}^{-1}$ greater during
4 days following the major rain event (i.e., during days 230-243) when antecedent conditions were
5 considered. Moreover, the incorporation of antecedent effects led to a longer delay between the
6 timing of the major rain event and the maximum R_{soil} , which occurred ~ 5 days later than when
7 only current conditions were considered (Fig. 2a vs. 2b). As a result, total growing season R_{soil}
8 was $\sim 15\%$ higher under the *Ctrl-ant* scenario (e.g., 571 gC m^{-2} under NSS assumptions, Fig. 2b)
9 compared to the *Ctrl* scenario (e.g., 498 gC m^{-2} under NSS, Fig. 2a). This increase in predicted
10 R_{soil} under the *Ctrl-ant* scenario for days 230-243 was primarily driven by greater root respiration
11 (Fig. 2a vs 2b).

12 **3.2 Effects of soil texture**

13 Varying soil texture resulted in the greatest difference in daily R_{soil} between the DETECT and
14 SS-DETECT models; however, integrated over the growing season, these differences were very
15 small (Fig. 3a,b,c). In particular, total growing season R_{soil} predicted by SS-DETECT was $\sim 1.5\%$
16 less than predicted by DETECT for soils consisting primarily of sand and silt (*ST-Sa* and *ST-Si*
17 scenarios; Fig. 3a,b), but was $\sim 3.3\%$ less for a clay dominated soil (*ST-Cl* scenario; Fig. 3c red
18 versus grey bars). These differences in R_{soil} under NSS versus SS assumptions were
19 approximately the same for the scenarios involving antecedent effects (Figs. 3d,e,f). Despite the
20 minor differences at the growing season scale, notable differences emerged at the daily scale.
21 For example, with the largest precipitation event of the year and the 10 days that followed (days
22 218-248), daily R_{soil} predicted by the DETECT model was on average $\sim 2.5\%$ less than daily R_{soil}
23 from the SS-DETECT model for the *ST-Sa* and *ST-Si* scenarios (Fig. S1). R_{soil} from DETECT



1 was 4% greater than DETECT-SS R_{soil} for the *ST-Cl* scenario, but when antecedent variables
2 were included in the models, this difference increased to 10% (Figs. 3 and S1).

3 Soil texture also affected the magnitude of predicted R_{soil} compared to the control
4 scenarios, both with and without antecedent effects (*Ctrl-ant* and *Ctrl*, respectively). In
5 particular, we found that total growing season R_{soil} , whether from the DETECT or the SS-
6 DETECT model, was ~30% and ~60% higher for the *ST-Si* and *ST-Cl* scenarios relative to the
7 *Ctrl* scenario (Figs. 3b, 3c, 4a). The change in R_{soil} was negligible, however, when the sand
8 content was increased from 60% (*Ctrl*) to 80% (*ST-Sa*) for both models (Fig. 3a, Fig. 4a). The
9 antecedent versions of the fine-textured scenarios (*ST-Si-ant* and *ST-Cl-ant*) resulted in ~45%
10 and ~95% increases in total growing season R_{soil} , respectively, compared to the *Ctrl-ant* scenario
11 (Figs. 3e, 3f, 4b). Greater root respiration (Figs. 3e,f), following the end of the second
12 precipitation period between days 230 and 245, primarily drove the larger percentage increases
13 for the *SL-Si-ant* and *SL-Cl-ant* scenarios compared to the non-antecedent versions (Fig. 4b vs
14 Fig. 4a; Fig. 4e).

15 3.3 Effects of precipitation regimes

16 Based on the four different precipitation scenarios that we explored in the context of the control
17 soil texture (sandy clay loam), varying the timing, frequency, or magnitude of precipitation led to
18 little difference between R_{soil} predicted by the DETECT and SS-DETECT models (Fig. S2).
19 However, the precipitation regime did affect the magnitude of R_{soil} predicted under NSS or SS
20 conditions. For example, total growing season R_{soil} predicted under the alternative precipitation
21 scenarios was lower relative to the *Ctrl* scenario. This decrease was relatively small (5-10%) for
22 the non-antecedent versions of the models (Fig. 4c), but was comparatively larger (15-22%) for
23 the antecedent versions (Fig. 4d). This reduction appears to be driven by the amount of time



1 over which daily R_{soil} responded to the second precipitation period, which occurred around day
2 220, 190, and 250 in the *Ctrl*, *P-E*, and *P-L* scenarios, respectively. Following this precipitation
3 event, daily R_{soil} achieved values around $10 \text{ g C m}^{-2} \text{ day}^{-1}$ for about 20 days in the *Ctrl* scenario
4 (Fig. 2a, days 220-240), but for only about five days in the *P-E* and *P-L* scenarios (Fig S2a,b,
5 after days 190 and 250, respectively). Increasing the frequency of precipitation while retaining
6 approximately the same annual amount (i.e., scenario *P-FM*) resulted in daily R_{soil} being
7 consistently less than that of the *Ctrl* scenario, which led to a reduction in total growing season
8 R_{soil} in the *P-FM* scenario (Fig. S2c and S2e).

9 **3.4 Effects of antecedent responses**

10 When antecedent soil water content and soil temperature were included in the DETECT model
11 we found that predicted R_{soil} was 15% greater for the control scenario and 29-37% greater for the
12 fine textured soil scenarios, compared to the corresponding scenarios that did not include
13 antecedent conditions. When the sand content was 80% or for any of the different precipitation
14 regimes, there was a negligible difference between R_{soil} predicted by the antecedent versus non-
15 antecedent parametrizations of DETECT.

16 Daily R_{soil} predicted by the DETECT model based on the *Ctrl* and *Ctrl-ant* scenarios
17 agreed well with observed ecosystem respiration (R_{eco}), but R_{eco} was slightly higher than
18 predicted R_{soil} (Fig. 2a,b), which was expected since $R_{eco} = R_{soil} +$ aboveground autotrophic
19 respiration. For the most part, this data-model agreement was similar whether the antecedent
20 model terms were included (Fig. 2b) or not (Fig. 2a). Unfortunately, R_{eco} data were not available
21 during the time period (days 230-250) associated with the greatest disagreement between the *Ctrl*
22 and *Ctrl-ant* scenarios. During this period, frequent hourly measurements of soil $[\text{CO}_2]$ were in
23 better agreement with predicted soil CO_2 from the *Ctrl-ant* scenario compared to the *Ctrl*



1 scenario (Fig. 5a,b, S3a,b). After day ~250, based on the DETECT model, both scenarios (*Ctrl*
2 and *Ctrl-ant*) under-predicted the observed soil [CO₂] by ~ 50% (Fig. 5).

3 **4. Discussion**

4 The DETECT and SS-DETECT models provide a framework for evaluating the circumstances
5 under which steady-state (SS) assumptions of soil CO₂ production and surface soil respiration
6 (R_{soil}) are valid, and to identify the major physical (i.e., soil texture, soil moisture) and/or
7 biological (i.e., root and microbial respiration responses) factors that lead to non-steady-state
8 (NSS) conditions.

9 **4.1 Steady-state versus non-steady-state conditions**

10 At the seasonal scale, there was reasonable agreement between total growing season R_{soil}
11 predicted under the assumption of SS versus NSS conditions, but the strength of this agreement
12 depended on soil texture (see §4.2). At the daily scale, R_{soil} predicted by the DETECT model
13 deviated from values expected under the assumption of SS conditions for 11 days or 4% of the
14 days during the April-September growing season (Fig 2, days 218-228). These discrepancies,
15 attributed to NSS conditions, were generally limited to periods following large rain events. For
16 applications that assume SS conditions, such as isotopic partitioning studies (Hui and Luo, 2004;
17 Ogle and Pendall, 2015), the SS assumption seemed reasonable during periods of minimal or no
18 precipitation, representative of times during which soil water content changes very little or
19 gradually. For sites or time periods characterized by pulsed precipitation patterns, our results
20 suggested that NSS conditions would be more likely over longer periods of time.

21 **4.2 Effect of varying soil texture**

22 Our results indicated that soil texture exerts the strongest control over the prevalence of NSS soil



1 CO₂ conditions. For a predominantly (e.g., 60%) sandy or silty soil, soil CO₂ transport and efflux
2 generally aligned with the SS assumption (Fig. 2, Fig. 3a-b). This was consistent with previous
3 work that used SS models to predict R_{soil} for similar soil types (Baldocchi et al., 2006; Vargas et
4 al., 2010).

5 For very fine-texture soil dominated by clay, however, SS assumptions were far less
6 appropriate. The larger difference in R_{soil} predicted under SS versus NSS conditions for fine-
7 texture (i.e., 60% clay) soil was apparent at both the growing season scale and the daily scale
8 following a large precipitation event (Fig. 3c,e, from day 218). In general, the DETECT model
9 predicted that R_{soil} should be higher in clay compared to sandy soil after precipitation events, a
10 result supported by field experiments (Cable et al., 2008), but this texture effect is muted under
11 assumptions of SS. Moreover, recovery of R_{soil} to SS rates after a large rain event took ~30 days
12 in the clay soil (Fig. 3c, days 218 to 248) compared to ~10 days for the other coarser soil texture
13 scenarios (Fig. 2, Fig. 3a-b, days 218 to ~230). These effects of soil texture on the prevalence of
14 NSS conditions can be attributed to soil physical properties and their effects on air-filled porosity
15 and CO₂ diffusivity. Fine textured soils have smaller pores and tend to retain water for longer
16 (Bouma and Bryla, 2000), which has the effect of decreasing soil CO₂ diffusivity (Fig. 6). Thus,
17 under moist conditions that follow a rain event, it may take 15 minutes or so for a CO₂ molecule
18 produced at 0.5 m to diffuse to the surface in a clay soil compared to only 1-2 minutes for a
19 sandy soil. Moreover, fine-textured soils have slower infiltration rates (Hillel, 1998), delaying
20 the exposure of more deeply distributed roots and microbes to increased moisture availability.
21 While this effect may not directly impact the SS assumption, it would lead to greater time lags
22 between precipitation pulses and R_{soil} peaks.



1 These findings have important implications for studies that rely on the SS assumption to
2 predict subsurface soil CO₂ production. The SS assumption may be sufficient for systems
3 defined by coarse-textured soils, but it may lead to erroneous conclusions if applied to fine-
4 textured soils. Our simulation experiments made the simplifying assumption that soil texture is
5 constant with depth, but in many ecosystems, texture may vary greatly with depth (Ogle et al.,
6 2004). An important next step is to extend the simulations to explore the impacts of depth-
7 varying soil texture on SS versus NSS conditions. The DETECT model can easily accommodate
8 such modifications; allowing soil texture to vary by depth would have a direct effect on soil
9 water content, which is simulated outside of DETECT using HYDRUS (Chou et al., 2008; Piao
10 et al., 2009; Šimůnek et al., 2008), that can accommodate such depth variation.

11 **4.3 Effect of varying the timing or frequency of precipitation**

12 Unlike soil texture, varying the timing, frequency, and magnitude of precipitation resulted in
13 predicted R_{soil} that was almost identical under SS and NSS assumptions, both at the growing
14 season and daily time-scales (Fig. S2). We had anticipated that such changes in the precipitation
15 regime would impact SS conditions via impacts on soil air-filled porosity and potentially by
16 changing the covariance between soil water and soil temperature, both of which affect soil CO₂
17 diffusivity (e.g., see Eqn 2). We did not explore, however, the effect of decreasing the frequency
18 while simultaneously increasing the magnitude of individual pulses. We hypothesize that this
19 latter scenario could produce more exaggerated or extended NSS conditions given that large rain
20 events would infiltrate deeper, reducing CO₂ diffusivity across greater soil depths, thus slowing
21 the transport of more deeply derived CO₂. Increasing the number of small events, as done in the
22 *P-FM* scenario, would generally confine water inputs to shallow layers, from which CO₂ has



1 shorter distances to travel to reach the surface, creating less opportunity for R_{soil} to exhibit NSS
2 behavior.

3 While the precipitation regimes that we explored (Table 3) did not notably impact SS
4 versus NSS behavior, they did influence the magnitude of growing season R_{soil} , with the
5 alternative regimes resulting in a decrease in growing season R_{soil} between 6% and 11%
6 compared to the control scenario (Fig 4c,d, Fig. S2). The decrease in R_{soil} as a result of
7 increasing the frequency while decreasing the magnitude of precipitation (*P-FM* and *P-FM-ant*
8 scenarios) is consistent with previous research (Borken and Matzner, 2009; Cable et al., 2008;
9 Huxman et al., 2004; Ogle et al., 2015; Schwinning et al., 2004; Sponseller, 2007). For example,
10 Cable et al. (2008) found that soil respiration is insensitive to small precipitation pulses (<7mm
11 in size), while Borken and Matzner (2009) found that an increase in the drying and wetting
12 frequency reduced the cumulative C mineralization. Likewise, shifting precipitation to one
13 month later (*P-L* scenario), which resulted in an abundance of rainfall at the end of the growing
14 season, resulted in lower growing season R_{soil} . In contrast, Chou et al. (2008) found that
15 abundant end of growing season precipitation increased growing season R_{soil} (Fig. 4c,d; Fig.
16 S2b,e). These differences in findings could be due to a number of reasons, such as dissimilar
17 daily precipitation patterns, different study systems, and different approaches to quantifying R_{soil} .
18 In Chou et al. (2008), the late season precipitation in one year allowed soil water content to
19 remain high for longer, resulting in high growing season R_{soil} compared to a different year with
20 greater overall annual precipitation but without the late surge in precipitation. In our analysis,
21 precipitation in the study year (2008) was concentrated in two relatively short time windows, and
22 thus, our scenarios are not directly comparable to those observed by Chou et al. (2008). Our
23 analysis could be extended, however, by exploring the impacts of more varied precipitation



1 regimes; given the flexibility of simulation approaches, we could use the DETECT model to
2 explicitly evaluate R_{soil} responses to any particular observed or hypothetical precipitation regime.

3 **4.4 Effect of antecedent conditions**

4 The inclusion or exclusion of antecedent soil moisture and temperature effects on CO_2
5 production rates had little to no impact on the balance between SS versus NSS behavior of R_{soil} .
6 However, incorporating antecedent effects generally increased the magnitude of R_{soil} as
7 microbial respiration was stimulated more during the initial onset of the main precipitation
8 period when antecedent effects were considered (Fig. 2b vs Fig 2a, day 218, blue line). This is
9 expected because the instantaneous response of microbes to a rain event is expected to be greater
10 following a dry period compared to during a wet period (Cable et al., 2013; Cable et al., 2008;
11 Sponseller, 2007; Thomas et al., 2008; Xu et al., 2004). These dynamics are incorporated in the
12 antecedent version of the models when the parameter corresponding to the interaction between
13 current and antecedent soil water content is negative (e.g., α_3 , Table 1). Secondly, root
14 respiration was greatly enhanced following the end of this period of precipitation (Fig. 2b vs Fig.
15 2a, days ~230-250, green line), despite there being little precipitation after day 230 (Fig. 2b).
16 This likely occurred because our DETECT model assumed that soil water over relatively longer
17 time periods (past 1-2 weeks, Eqn. 12) affects current root respiration rates. This partly reflects
18 the mechanism that roots are able to take up more soil water that has infiltrated to deeper depths
19 (Cable et al., 2013). The microbes, however, are coupled to past conditions over comparatively
20 short time periods (a couple days).

21 The importance and benefit of including antecedent terms for modelling soil respiration
22 or ecosystem respiration has been well documented (Barron-Gafford et al., 2014; Cable et al.,
23 2013; Ryan et al., 2015). Thus, we encourage future studies to include influences of past



1 conditions when modelling subsurface and surface CO₂ fluxes. Fortunately, our simulation
2 experiments suggest that the lagged responses of microbial and root respiration to soil moisture
3 and temperature do not have a notable impact on the SS assumption.

4 **4.4 Comparison of modelled soil CO₂ with data**

5 The good agreement between modeled and observed soil CO₂ concentrations—particularly when
6 including antecedent effects—was very encouraging because the DETECT model was not
7 rigorously tuned or calibrated to fit data on soil [CO₂] or ecosystem CO₂ fluxes (R_{eco}) (Figs. 5,
8 S3). However, there remained discrepancies between the predicted and observed CO₂ fluxes,
9 particularly after rain events. These discrepancies could be an artifact of the input data used to
10 calculate CO₂ production (i.e., the source term). Some parameter values were drawn from the
11 literature and others were estimated by fitting a non-linear regression model to data. For
12 example, the parameters describing the current and antecedent soil water content effects (α 's)
13 were obtained by fitting a non-linear model to R_{eco} data (Ryan et al., 2015). While measured R_{eco}
14 represents both root respiration and microbial respiration contributions, it also reflects
15 aboveground respiration, which is not currently treated in the DETECT model. Moreover, we
16 made further assumptions about how the R_{eco} parameter estimates translate to component
17 processes (root and microbial responses), and we relied on literature information about how
18 microbes and roots respond to precipitation events (e.g., the timing, magnitude, and lags). Future
19 studies could rigorously fit the DETECT model to field data, such as observations of R_{soil} , soil
20 CO₂ concentrations, and ¹³C isotope fluxes. Using a Bayesian methodology to do this would
21 allow one to incorporate multiple data sets to inform all parameters in DETECT.

22 **4.5 Non-steady state model of soil CO₂ transport and production**

23 An important contribution of this this study was the development of a non-steady state (NSS)



1 model of soil CO₂ transport and production (the DETECT model version 1.0), which is
2 particularly useful for systems that may frequently experience NSS conditions. Other comparable
3 NSS models exist (e.g., Fang and Moncrieff, 1999; Hui and Luo, 2004; Šimůnek and Suarez,
4 1993), but they generally treat the production (source) terms—root/rhizosphere respiration and
5 microbial decomposition of soil organic matter—simplistically, and accompanying model code
6 is not available. Our DETECT v1.0 model includes more detailed submodels for the production
7 terms, inspired by recent studies (E.g. Carrillo et al., 2014a; Davidson et al., 2012; Lloyd and
8 Taylor, 1994; Pendall et al., 2003; Todd-Brown et al., 2012); in contrast to these studies, which
9 essentially described models for “bulk” soil, we applied the CO₂ production models to every
10 depth increment. Additionally, we have provided model code, implemented in Matlab (see *Code*
11 *Availability* section), with the goal of making the DETECT model, and ability to accommodate
12 NSS conditions, more accessible to potential users.

13 **5. Conclusions**

14 Determining the conditions under which steady-state (SS) assumptions are appropriate for
15 modeling soil CO₂ production, transport, and efflux is crucial for accurately modeling the
16 contribution of soils to the carbon cycle. We found that soil texture exerted the greatest control
17 over whether SS assumptions are appropriate. When the soil at a site is coarse (60% or more
18 sand), SS assumptions appeared to be appropriate, and one could apply a simpler, more
19 computationally efficient SS model, such as SS-DETECT (see also Amundson et al., 1998). As
20 the soil texture becomes increasingly finer, SS assumptions start to break down, especially
21 following large precipitation events that can greatly impact soil water content and associated soil
22 air-filled porosity, thus affecting CO₂ diffusivity. Under such conditions, the more complex and
23 computationally demanding NSS model (DETECT) is preferred. We found that precipitation



1 regime characteristics and/or the inclusion of antecedent soil moisture and temperature
2 conditions had little singular effect on whether SS or NSS assumptions were appropriate.
3 However, while these factors do not directly impact SS versus NSS behavior, they were found to
4 be important for accurately modeling the soil carbon cycle because they notably impacted the
5 magnitude of the soil CO₂ efflux.

6 **Code availability**

7 All of the Matlab script files for running the DETECT model can be accessed via
8 <http://doi.org/10.5281/zenodo.927501>. These Matlab script files are set up so that the model
9 runs at the PHACE field site. The above weblink also provides a user manual which gives
10 instructions for running DETECT at either the PHACE site or at a user specified field site. We
11 also provide Matlab script files for creating a time series of predicted versus observed soil
12 respiration (figure 1) and a time series of predicted versus observed soil CO₂ (figure 5). These
13 can be found via <http://doi.org/10.5281/zenodo.927313>. Following publication, these Matlab
14 files and the data files (see next section) will be available to download from the Ogle lab website
15 via <http://jan.ucc.nau.edu/ogle-lab/>.

16 **Data availability**

17 Measurement data made at the PHACE field site, which are required as inputs for the DETECT
18 model, are available via <http://doi.org/10.5281/zenodo.926064>.

19 **Acknowledgements**

20 We thank Dan LeCain, David Smith, and Erik Hardy for implementing and managing the
21 PHACE experiment, and Jack Morgan for project leadership. This material is based upon work
22 supported by the US Department of Agriculture Agricultural Research Service Climate Change,



1 Soils & Emissions Program, USDA-CSREES Soil Processes Program (#2008-35107-18655), US
2 Department of Energy Office of Science (BER), through the Terrestrial Ecosystem Science
3 program (#DE-SC0006973) and the Western Regional Center of the National Institute for
4 Climatic Change Research, and by the National Science Foundation (DEB#1021559). Any
5 opinions, findings, and conclusions or recommendations expressed in this material are those of
6 the author(s) and do not necessarily reflect the views of the National Science Foundation.

7

8 **References**

- 9 Amundson, R., Stern, L., Baisden, T., and Wang, Y.: The isotopic composition of soil and soil-
10 respired CO₂, *Geoderma*, 82, 83-114, 1998.
- 11 Atkin, O. K. and Tjoelker, M. G.: Thermal acclimation and the dynamic response of plant
12 respiration to temperature, *Trends in plant science*, 8, 343-351, 2003.
- 13 Bachman, S., Heisler-White, J. L., Pendall, E., Williams, D. G., Morgan, J. A., and Newcomb, J.:
14 Elevated carbon dioxide alters impacts of precipitation pulses on ecosystem photosynthesis and
15 respiration in a semi-arid grassland, *Oecologia*, 162, 791-802, 2010.
- 16 Baldocchi, D., Tang, J., and Xu, L.: How switches and lags in biophysical regulators affect
17 spatial-temporal variation of soil respiration in an oak-grass savanna, *Journal of Geophysical*
18 *Research: Biogeosciences* (2005–2012), 111, 2006.
- 19 Barron-Gafford, G. A., Cable, J. M., Bentley, L. P., Scott, R. L., Huxman, T. E., Jenerette, G. D.,
20 and Ogle, K.: Quantifying the timescales over which exogenous and endogenous conditions
21 affect soil respiration, *New Phytologist*, 202, 442-454, 2014.
- 22 Birch, H.: The effect of soil drying on humus decomposition and nitrogen availability, *Plant and*
23 *Soil*, 10, 9-31, 1958.
- 24 Boroken, W., Davidson, E., Savage, K., Gaudinski, J., and Trumbore, S. E.: Drying and wetting
25 effects on carbon dioxide release from organic horizons, *Soil Science Society of America*
26 *Journal*, 67, 1888-1896, 2003.
- 27 Boroken, W. and Matzner, E.: Reappraisal of drying and wetting effects on C and N
28 mineralization and fluxes in soils, *Global change biology*, 15, 808-824, 2009.
- 29 Bouma, T. J. and Bryla, D. R.: On the assessment of root and soil respiration for soils of different
30 textures: interactions with soil moisture contents and soil CO₂ concentrations, *Plant and Soil*,
31 227, 215-221, 2000.
- 32 Brennan, A.: Vegetation and Climate Change Alter Ecosystem Carbon Losses at the Prairie
33 Heating and CO₂ Enrichment Experiment in Wyoming, Department of Botany, University of
34 Wyoming, 2013.



- 1 Cable, J. M., Ogle, K., Barron-Gafford, G. A., Bentley, L. P., Cable, W. L., Scott, R. L.,
2 Williams, D. G., and Huxman, T. E.: Antecedent conditions influence soil respiration differences
3 in shrub and grass patches, *Ecosystems*, 16, 1230-1247, 2013.
- 4 Cable, J. M., Ogle, K., Lucas, R. W., Huxman, T. E., Loik, M. E., Smith, S. D., Tissue, D. T.,
5 Ewers, B. E., Pendall, E., and Welker, J. M.: The temperature responses of soil respiration in
6 deserts: a seven desert synthesis, *Biogeochemistry*, 103, 71-90, 2011.
- 7 Cable, J. M., Ogle, K., Williams, D. G., Weltzin, J. F., and Huxman, T. E.: Soil texture drives
8 responses of soil respiration to precipitation pulses in the Sonoran Desert: implications for
9 climate change, *Ecosystems*, 11, 961-979, 2008.
- 10 Carrillo, Y., Dijkstra, F. A., LeCain, D., Morgan, J. A., Blumenthal, D., Waldron, S., and
11 Pendall, E.: Disentangling root responses to climate change in a semiarid grassland, *Oecologia*,
12 1-13, 2014a.
- 13 Carrillo, Y., Dijkstra, F. A., Pendall, E., LeCain, D., and Tucker, C.: Plant rhizosphere influence
14 on microbial C metabolism: the role of elevated CO₂, N availability and root stoichiometry,
15 *Biogeochemistry*, 117, 229-240, 2014b.
- 16 Carrillo, Y. and Pendall, E.: Combined effects of elevated CO₂ and warming on soil carbon and
17 microbial C use, in review.
- 18 Chou, W. W., Silver, W. L., Jackson, R. D., Thompson, A. W., and ALLEN-DIAZ, B.: The
19 sensitivity of annual grassland carbon cycling to the quantity and timing of rainfall, *Global
20 Change Biology*, 14, 1382-1394, 2008.
- 21 Cox, P. M.: Description of the TRIFFID dynamic global vegetation model, 2001.
- 22 Davidson, E. A. and Janssens, I. A.: Temperature sensitivity of soil carbon decomposition and
23 feedbacks to climate change, *Nature*, 440, 165-173, 2006.
- 24 Davidson, E. A., Samanta, S., Caramori, S. S., and Savage, K.: The Dual Arrhenius and
25 Michaelis–Menten kinetics model for decomposition of soil organic matter at hourly to seasonal
26 time scales, *Global Change Biology*, 18, 371-384, 2012.
- 27 Fang, C. and Moncrieff, J. B.: A model for soil CO₂ production and transport 1.: Model
28 development, *Agricultural and Forest Meteorology*, 95, 225-236, 1999.
- 29 Friedlingstein, P., Andrew, R. M., Rogelj, J., Peters, G., Canadell, J. G., Knutti, R., Luderer, G.,
30 Raupach, M. R., Schaeffer, M., and Van Vuuren, D. P.: Persistent growth of CO₂ emissions and
31 implications for reaching climate targets, *Nature geoscience*, 7, 709, 2014.
- 32 Haberman, R.: Elementary applied partial differential equations (Third Edition), Prentice Hall
33 Englewood Cliffs, NJ, 1998.
- 34 Hanson, P., Edwards, N., Garten, C., and Andrews, J.: Separating root and soil microbial
35 contributions to soil respiration: a review of methods and observations, *Biogeochemistry*, 48,
36 115-146, 2000.
- 37 Hashimoto, S., Carvalhais, N., Ito, A., Migliavacca, M., Nishina, K., and Reichstein, M.: Global
38 spatiotemporal distribution of soil respiration modeled using a global database, *Biogeosciences*,
39 12, 4121-4132, 2015.



- 1 Hillel, D.: Environmental soil physics: Fundamentals, applications, and environmental
2 considerations, Academic press, 1998.
- 3 Hui, D. and Luo, Y.: Evaluation of soil CO₂ production and transport in Duke Forest using a
4 process-based modeling approach, *Global Biogeochemical Cycles*, 18, 2004.
- 5 Huxman, T. E., Snyder, K. A., Tissue, D., Leffler, A. J., Ogle, K., Pockman, W. T., Sandquist,
6 D. R., Potts, D. L., and Schwinning, S.: Precipitation pulses and carbon fluxes in semiarid and
7 arid ecosystems, *Oecologia*, 141, 254-268, 2004.
- 8 Jarvis, P., Rey, A., Petsikos, C., Wingate, L., Rayment, M., Pereira, J., Banza, J., David, J.,
9 Miglietta, F., and Borghetti, M.: Drying and wetting of Mediterranean soils stimulates
10 decomposition and carbon dioxide emission: the “Birch effect”, *Tree physiology*, 27, 929-940,
11 2007.
- 12 Jasoni, R. L., Smith, S. D., and Arnone, J. A.: Net ecosystem CO₂ exchange in Mojave Desert
13 shrublands during the eighth year of exposure to elevated CO₂, *Global Change Biology*, 11, 749-
14 756, 2005.
- 15 Kayler, Z. E., Sulzman, E. W., Rugh, W. D., Mix, A. C., and Bond, B. J.: Characterizing the
16 impact of diffusive and advective soil gas transport on the measurement and interpretation of the
17 isotopic signal of soil respiration, *Soil Biology and Biochemistry*, 42, 435-444, 2010.
- 18 Kemp, P. R., Reynolds, J. F., Pachepsky, Y., and Chen, J. L.: A comparative modeling study of
19 soil water dynamics in a desert ecosystem, *Water Resources Research*, 33, 73-90, 1997.
- 20 Lee, X., Wu, H. J., Sigler, J., Oishi, C., and Siccama, T.: Rapid and transient response of soil
21 respiration to rain, *Global Change Biology*, 10, 1017-1026, 2004.
- 22 Lloyd, J. and Taylor, J.: On the temperature dependence of soil respiration, *Functional ecology*,
23 315-323, 1994.
- 24 Luo, Y. and Zhou, X.: Soil respiration and the environment, Academic press, 2010.
- 25 Maggi, F. and Riley, W. J.: Transient competitive complexation in biological kinetic isotope
26 fractionation explains nonsteady isotopic effects: Theory and application to denitrification in
27 soils, *Journal of Geophysical Research: Biogeosciences*, 114, 2009.
- 28 Mathworks: The MathWorks, Inc. Natick, Massachusetts, USA MATLAB and Statistics
29 Toolbox Release 2016b. 2016.
- 30 Meisner, A., Bååth, E., and Rousk, J.: Microbial growth responses upon rewetting soil dried for
31 four days or one year, *Soil Biology and Biochemistry*, 66, 188-192, 2013.
- 32 Moldrup, P., Olesen, T., Yoshikawa, S., Komatsu, T., and Rolston, D. E.: Three-porosity model
33 for predicting the gas diffusion coefficient in undisturbed soil, *Soil Science Society of America
34 Journal*, 68, 750-759, 2004.
- 35 Morgan, J. A., LeCain, D. R., Pendall, E., Blumenthal, D. M., Kimball, B. A., Carrillo, Y.,
36 Williams, D. G., Heisler-White, J., Dijkstra, F. A., and West, M.: C₄ grasses prosper as carbon
37 dioxide eliminates desiccation in warmed semi-arid grassland, *Nature*, 476, 202-205, 2011.



- 1 Moyes, A. B., Gaines, S. J., Siegwolf, R. T., and Bowling, D. R.: Diffusive fractionation
2 complicates isotopic partitioning of autotrophic and heterotrophic sources of soil respiration,
3 *Plant, cell & environment*, 33, 1804-1819, 2010.
- 4 Mueller, K. E., Blumenthal, D. M., Pendall, E., Carrillo, Y., Dijkstra, F. A., Williams, D. G.,
5 Follett, R. F., and Morgan, J. A.: Impacts of warming and elevated CO₂ on a semi-arid grassland
6 are non-additive, shift with precipitation, and reverse over time, *Ecology letters*, 19, 956-966,
7 2016.
- 8 Nickerson, N. and Risk, D.: Physical controls on the isotopic composition of soil-respired CO₂,
9 *Journal of Geophysical Research: Biogeosciences* (2005–2012), 114, 2009.
- 10 Ogle, K., Barber, J. J., Barron-Gafford, G. A., Bentley, L. P., Young, J. M., Huxman, T. E., Loik,
11 M. E., and Tissue, D. T.: Quantifying ecological memory in plant and ecosystem processes,
12 *Ecology letters*, 18, 221-235, 2015.
- 13 Ogle, K. and Pendall, E.: Isotope partitioning of soil respiration: A Bayesian solution to
14 accommodate multiple sources of variability, *Journal of Geophysical Research: Biogeosciences*,
15 2015.
- 16 Ogle, K., Ryan, E., Dijkstra, F. A., and Pendall, E.: Quantifying and reducing uncertainties in
17 estimated soil CO₂ fluxes with hierarchical data-model integration, *Journal of Geophysical*
18 *Research: Biogeosciences*, 2016.
- 19 Ogle, K., Wolpert, R. L., and Reynolds, J. F.: Reconstructing plant root area and water uptake
20 profiles, *Ecology*, 85, 1967-1978, 2004.
- 21 Oikawa, P., Grantz, D., Chatterjee, A., Eberwein, J., Allsman, L., and Jenerette, G.: Unifying soil
22 respiration pulses, inhibition, and temperature hysteresis through dynamics of labile soil carbon
23 and O₂, *Journal of Geophysical Research: Biogeosciences*, 119, 521-536, 2014.
- 24 Oleson, K., Lawrence, D., Bonan, G., Drewniak, B., Huang, M., Koven, C., Levis, S., Li, F.,
25 Riley, W., and Subin, Z.: Technical description of version 4.5 of the Community Land Model
26 (CLM). Near Tech. Note NCAR/TN-503+ STR. National Center for Atmospheric Research,
27 Boulder, CO, 422 pp. doi: 10.5065/D6RR1W7M., 2013.
- 28 Pendall, E., Bridgham, S., Hanson, P. J., Hungate, B., Kicklighter, D. W., Johnson, D. W., Law,
29 B. E., Luo, Y., Megonigal, J. P., and Olsrud, M.: Below-ground process responses to elevated
30 CO₂ and temperature: A discussion of observations, measurement methods, and models, *New*
31 *Phytologist*, 162, 311-322, 2004.
- 32 Pendall, E., Del Grosso, S., King, J., LeCain, D., Milchunas, D., Morgan, J., Mosier, A., Ojima,
33 D., Parton, W., and Tans, P.: Elevated atmospheric CO₂ effects and soil water feedbacks on soil
34 respiration components in a Colorado grassland, *Global Biogeochemical Cycles*, 17, 2003.
- 35 Pendall, E., Heisler-White, J. L., Williams, D. G., Dijkstra, F. A., Carrillo, Y., Morgan, J. A., and
36 LeCain, D. R.: Warming reduces carbon losses from grassland exposed to elevated atmospheric
37 carbon dioxide, *PloS one*, 8, e71921, 2013.
- 38 Pendall, E., Leavitt, S. W., Brooks, T., Kimball, B. A., Pinter Jr, P. J., Wall, G. W., LaMorte, R.
39 L., Wechsung, G., Wechsung, F., and Adamsen, F.: Elevated CO₂ stimulates soil respiration in a
40 FACE wheat field, *Basic and Applied Ecology*, 2, 193-201, 2001.



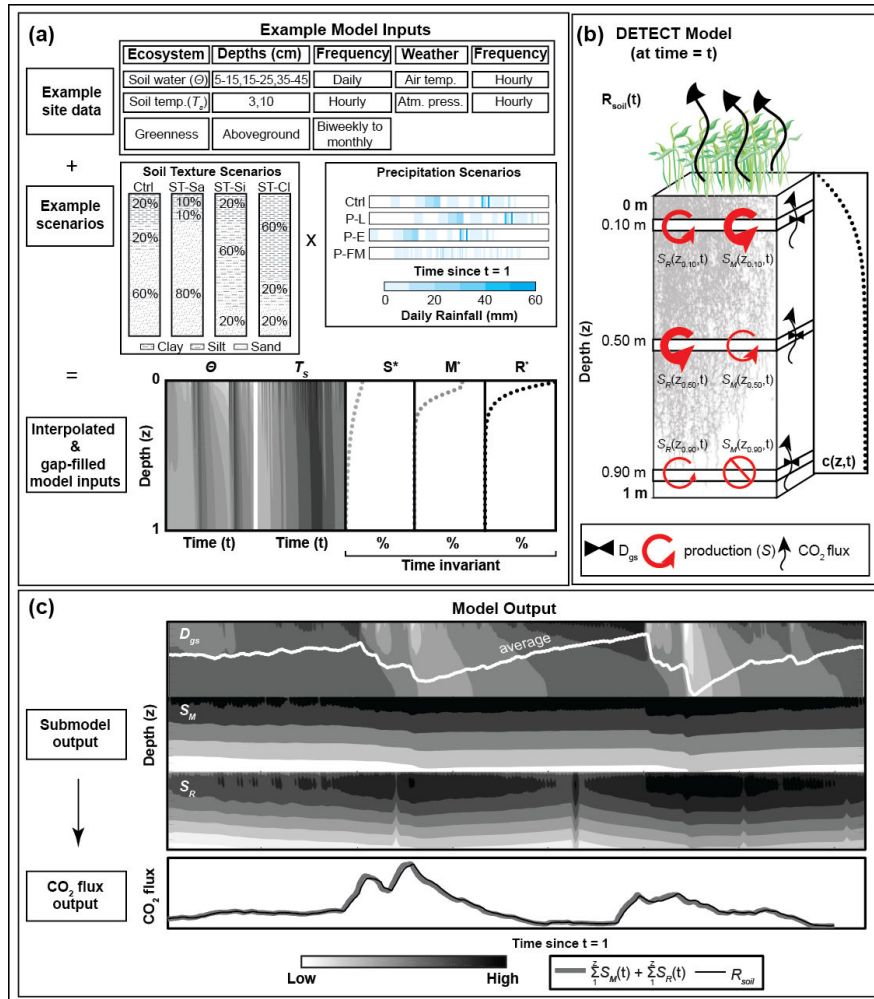
- 1 Piao, S., Ciais, P., Friedlingstein, P., de Noblet-Ducoudre, N., Cadule, P., and al., e.:
2 Spatiotemporal patterns of terrestrial carbon cycle during the 20th century, 23, 2009.
- 3 Reynolds, J. F., Kemp, P. R., Ogle, K., and Fernández, R. J.: Modifying the ‘pulse–
4 reserve’ paradigm for deserts of North America: precipitation pulses, soil water, and plant
5 responses, *Oecologia*, 141, 194-210, 2004.
- 6 Richards, L. A.: Capillary conduction of liquids through porous mediums, *Physics*, 1, 318-333,
7 1931.
- 8 Risk, D., Kellman, L., and Beltrami, H.: A new method for in situ soil gas diffusivity
9 measurement and applications in the monitoring of subsurface CO₂ production, *Journal of*
10 *Geophysical Research: Biogeosciences*, 113, 2008.
- 11 Risk, D., Nickerson, N., Creelman, C., McArthur, G., and Owens, J.: Forced Diffusion soil flux:
12 A new technique for continuous monitoring of soil gas efflux, *Agricultural and forest*
13 *meteorology*, 151, 1622-1631, 2011.
- 14 Risk, D., Nickerson, N., Phillips, C., Kellman, L., and Moroni, M.: Drought alters respired δ^{13}
15 CO₂ from autotrophic, but not heterotrophic soil respiration, *Soil Biology and Biochemistry*, 50,
16 26-32, 2012.
- 17 Ryan, E. M., Ogle, K., Zelikova, T. J., LeCain, D. R., Williams, D. G., Morgan, J. A., and
18 Pendall, E.: Antecedent moisture and temperature conditions modulate the response of
19 ecosystem respiration to elevated CO₂ and warming, *Global Change Biology*, 2015.
- 20 Sala, O., Lauenroth, W., and Parton, W.: Long-Term Soil Water Dynamics in the Shortgrass
21 Steppe, *Ecology*, 73, 1175-1181, 1992.
- 22 Sala, O. E., Lauenroth, W., Parton, W., and Trlica, M.: Water status of soil and vegetation in a
23 shortgrass steppe, *Oecologia*, 48, 327-331, 1981.
- 24 Schwinning, S., Sala, O. E., Loik, M. E., and Ehleringer, J. R.: Thresholds, memory, and
25 seasonality: understanding pulse dynamics in arid/semi-arid ecosystems, *Oecologia*, 141, 191-
26 193, 2004.
- 27 Šimůnek, J. and Suarez, D. L.: Modeling of carbon dioxide transport and production in soil: 1.
28 Model development, *Water Resources Research*, 29, 487-497, 1993.
- 29 Simunek, J., Van Genuchten, M. T., and Sejna, M.: The HYDRUS-1D software package for
30 simulating the one-dimensional movement of water, heat, and multiple solutes in variably-
31 saturated media, *University of California-Riverside Research Reports*, 3, 1-240, 2005.
- 32 Šimůnek, J., van Genuchten, M. T., and Šejna, M.: Development and applications of the
33 HYDRUS and STANMOD software packages and related codes, *Vadose Zone Journal*, 7, 587-
34 600, 2008.
- 35 Šimůnek, J., Van Genuchten, M. T., and Šejna, M.: HYDRUS: Model use, calibration, and
36 validation, *Trans. Asabe*, 55, 1261-1274, 2012.
- 37 Sitch, S., Huntingford, C., Gedney, N., Levy, P., Lomas, M., Piao, S., Betts, R., Ciais, P., Cox,
38 P., and Friedlingstein, P.: Evaluation of the terrestrial carbon cycle, future plant geography and
39 climate-carbon cycle feedbacks using five Dynamic Global Vegetation Models (DGVMs),
40 *Global Change Biology*, 14, 2015-2039, 2008.



- 1 Sponseller, R. A.: Precipitation pulses and soil CO₂ flux in a Sonoran Desert ecosystem, *Global*
2 *Change Biology*, 13, 426-436, 2007.
- 3 Tang, J., Baldocchi, D. D., Qi, Y., and Xu, L.: Assessing soil CO₂ efflux using continuous
4 measurements of CO₂ profiles in soils with small solid-state sensors, *Agricultural and Forest*
5 *Meteorology*, 118, 207-220, 2003.
- 6 Thomas, A. D., Hoon, S. R., and Linton, P. E.: Carbon dioxide fluxes from cyanobacteria crusted
7 soils in the Kalahari, *Applied Soil Ecology*, 39, 254-263, 2008.
- 8 Todd-Brown, K. E., Hopkins, F. M., Kivlin, S. N., Talbot, J. M., and Allison, S. D.: A
9 framework for representing microbial decomposition in coupled climate models,
10 *Biogeochemistry*, 109, 19-33, 2012.
- 11 Tucker, C. L., Bell, J., Pendall, E., and Ogle, K.: Does declining carbon-use efficiency explain
12 thermal acclimation of soil respiration with warming?, *Global Change Biology*, 19, 252-263,
13 2013.
- 14 Vargas, R., Baldocchi, D. D., Allen, M. F., Bahn, M., Black, T. A., Collins, S. L., Yuste, J. C.,
15 Hirano, T., Jassal, R. S., and Pumpanen, J.: Looking deeper into the soil: biophysical controls
16 and seasonal lags of soil CO₂ production and efflux, *Ecological Applications*, 20, 1569-1582,
17 2010.
- 18 Vargas, R., Carbone, M. S., Reichstein, M., and Baldocchi, D. D.: Frontiers and challenges in
19 soil respiration research: from measurements to model-data integration, *Biogeochemistry*, 102,
20 1-13, 2011.
- 21 Xiang, S.-R., Doyle, A., Holden, P. A., and Schimel, J. P.: Drying and rewetting effects on C and
22 N mineralization and microbial activity in surface and subsurface California grassland soils, *Soil*
23 *Biology and Biochemistry*, 40, 2281-2289, 2008.
- 24 Xu, L., Baldocchi, D. D., and Tang, J.: How soil moisture, rain pulses, and growth alter the
25 response of ecosystem respiration to temperature, *Global Biogeochemical Cycles*, 18, 2004.
- 26 Zelikova, T. J., Williams, D. G., Hoenigman, R., Blumenthal, D. M., Morgan, J. A., and Pendall,
27 E.: Seasonality of soil moisture mediates responses of ecosystem phenology to elevated CO₂ and
28 warming in a semi-arid grassland, *Journal of Ecology*, 103, 1119-1130, 2015.
- 29
30
31
32
33
34
35
36
37
38

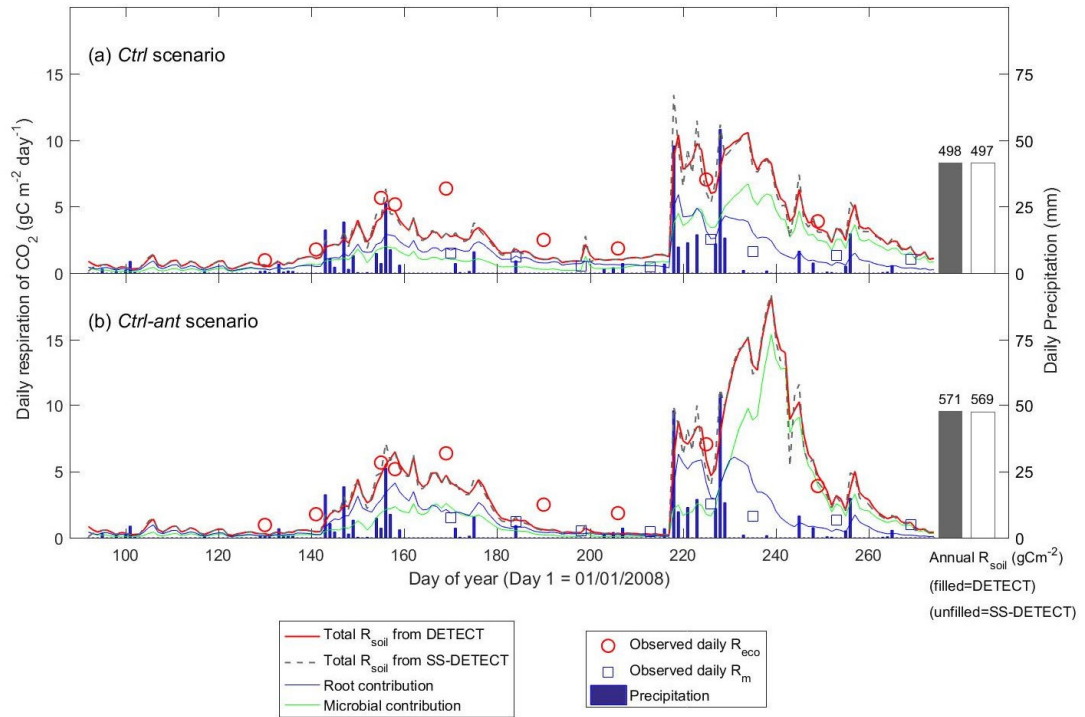


1 Figures



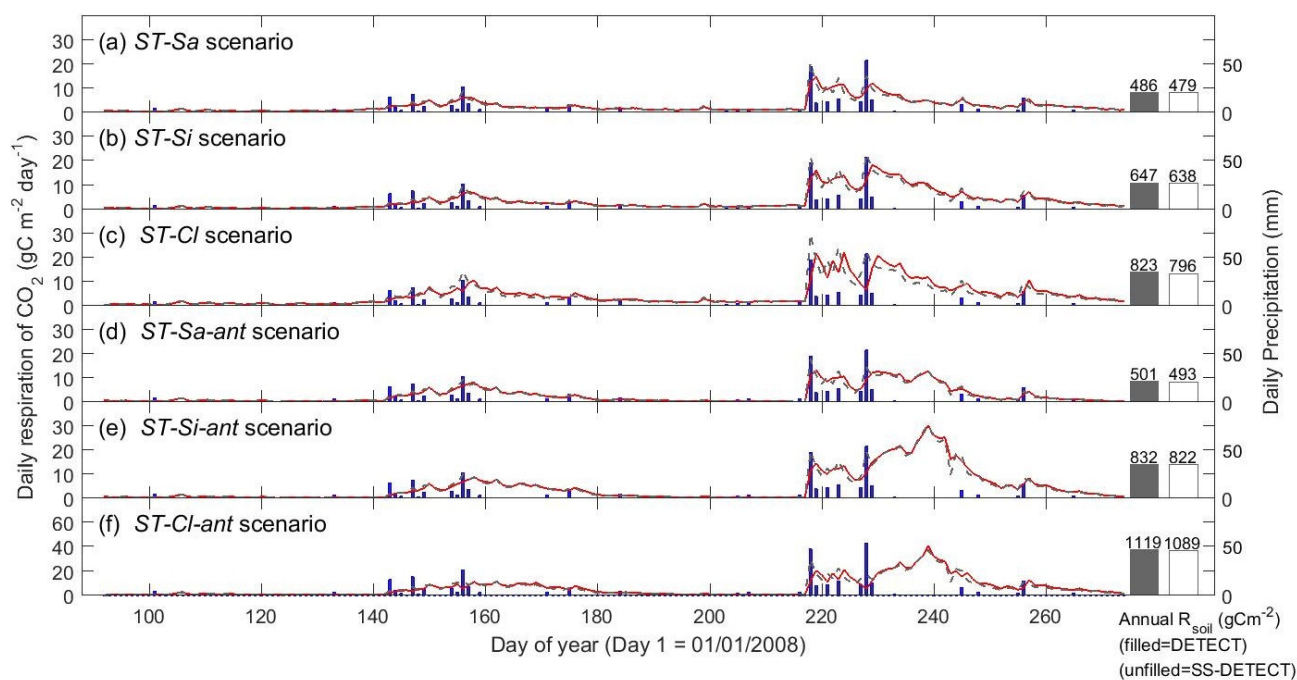
2

3 **Figure 1.** Graphical representation of (A) the required inputs to the DETECT model and the
 4 associated scenarios implemented in this study, (B) the components of the DETECT model at a
 5 particular time t , indicating depth-dependent production, CO₂ concentrations, and CO₂ fluxes,
 6 and (C) example model outputs, such as temporally and spatially varying CO₂ diffusivity and
 7 CO₂ production, and temporally varying bulk CO₂ fluxes. In this study, the model inputs in (A)
 8 include interpolated and gap-filled environmental drivers derived from field measurements
 9 (example from the Wyoming PHACE site) [Ryan *et al.*, 2015], combined with soil texture and
 10 precipitation scenarios. The gap-filled data drives the DETECT model in (B), which numerically
 11 solves for soil CO₂ at each depth z and time t given diffusivity and production submodels at each
 12 z and t , providing a complete picture of time- and depth-varying CO₂ production by microbes
 13 (S_M) and roots (S_R) production, diffusivity (D_{gs}), and bulk CO₂ fluxes as illustrated in (C).



1

2 **Figure 2** Time-series of daily surface soil CO₂ fluxes (R_{soil}) predicted by the non-steady-state (DETECT) and steady-state (SS-
 3 DETECT) models over the growing season (1st April – 30th September), based on the control scenarios (a) without (*Ctrl*) and (b) with
 4 (*Ctrl-ant*) antecedent effects (see Table 2). Only total R_{soil} is shown for the SS-DETECT model, whereas R_{soil} and its root and
 5 microbial contributions are shown for the DETECT model. The predicted fluxes are overlaid with observed ecosystem respiration
 6 (R_{eco} ; R_{soil} + aboveground plant respiration) and microbial respiration (R_m ; based on plots where vegetation was removed).

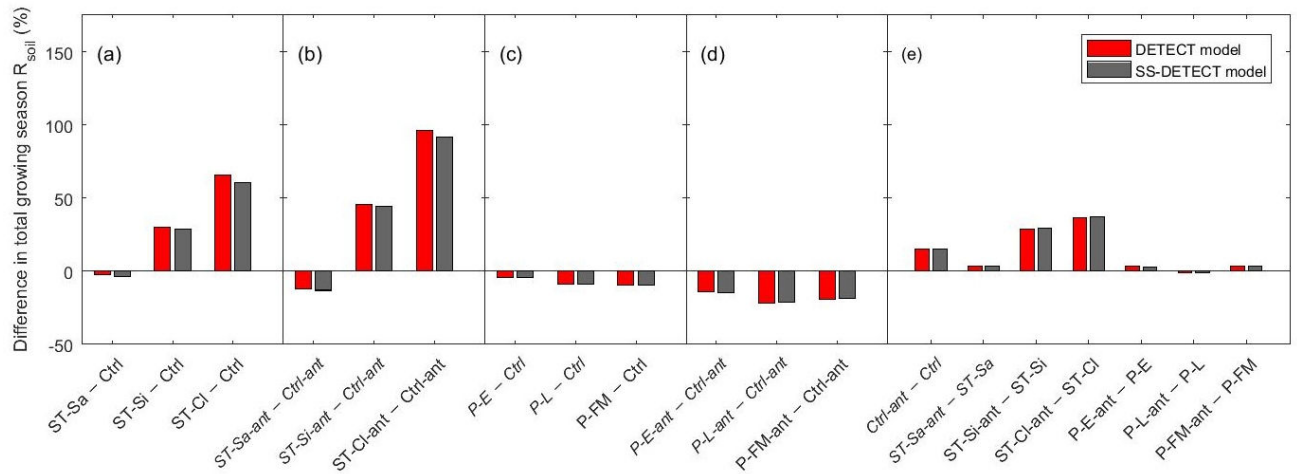


1

2 **Figure 3** Time-series of daily surface soil respiration (R_{soil}) predicted from the non-steady-state (NSS) DETECT model (red solid
 3 lines) and the steady-state (SS-DETECT) model (grey dashed lines), for different soil texture scenarios. The first three scenarios are
 4 the same as the control (*Ctrl*), except they assume a different soil texture: (a) more sandy soil, (b) more silty soil, or (c) more clayey
 5 soil. Panels (d), (e), and (f) show the R_{soil} predictions from the same soil texture scenarios as in (a)-(c), but also including antecedent
 6 effects of soil moisture and temperature. See Table 2 for descriptions of each scenario. R_{soil} predictions are overlaid with daily
 7 precipitation.



1

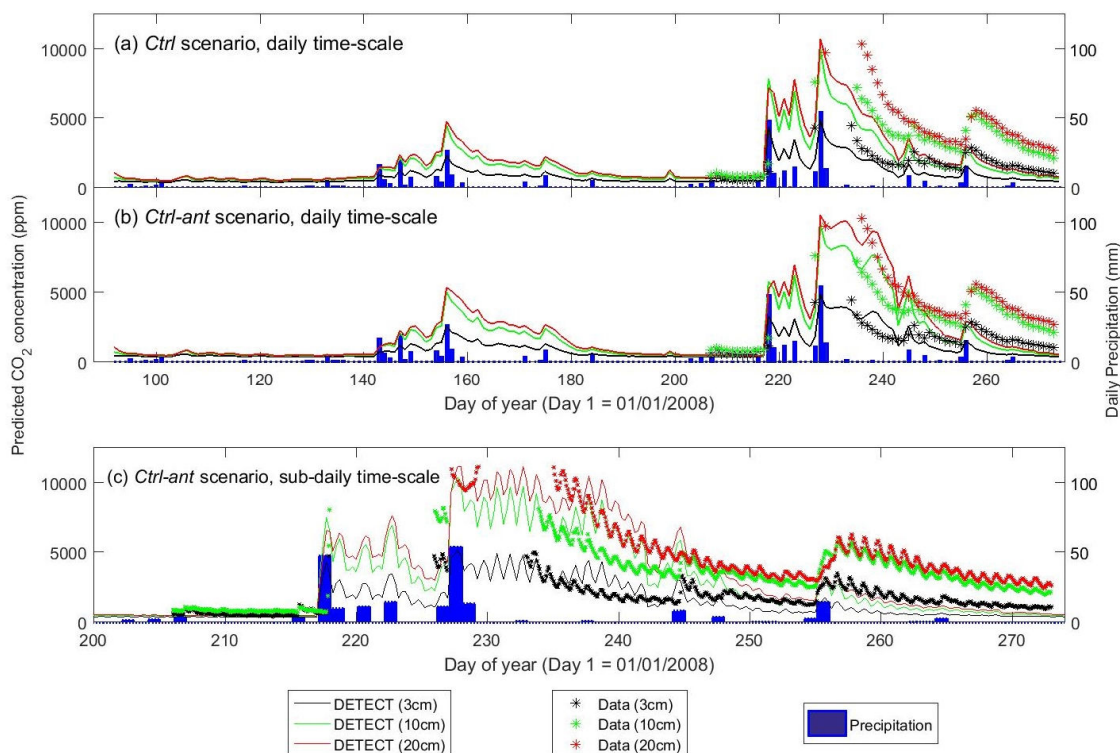


2

3 **Figure 4** Differences of total growing season (April-September) soil respiration (R_{soil}) as predicted by the non-steady-state (DETECT)
 4 and steady-state (SS-DETECT) models, for different pairs of scenarios. Comparisons are grouped such that they quantify the effects of
 5 (a) soil texture without antecedent effects, (b) soil texture with antecedent effects, (c) precipitation without antecedent effects, (d)
 6 precipitation with antecedent effects, and (e) antecedent effects. See Table 2 for descriptions of each scenario .

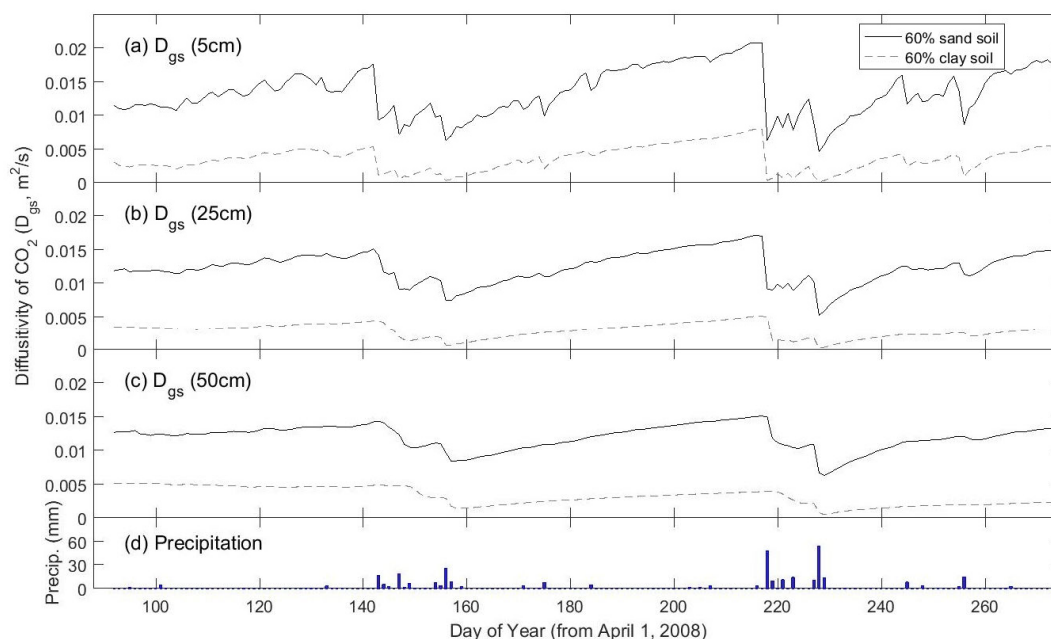
7

8



1

2 **Figure 5** Time-series of predicted versus observed soil CO₂ concentrations for depths 3 cm, 10 cm, and 20 cm, where the predictions
 3 are based on the non-steady-state (NSS) DETECT model. Predicted [CO₂] is shown for the daily time-scale for the control scenarios
 4 (a) without (*Ctrl*) and (b) with (*Ctrl-ant*) antecedent effects, and for (c) the subdaily (every 6 hours) time scale for the *Ctrl-ant*
 5 scenario. Units are in parts per million (ppm).



1

2

3 **Figure 6** Time series of how the modelled diffusivity of CO₂ (D_{gs}) at three different depths (5,
4 25, and 50 cm) varies between a predominantly sandy soil (solid line) and a predominantly clay
5 soil (dashed line). Predictions are from the non-steady state (DETECT) model for the *Ctrl* (60%
6 sand) and *ST-Cl* (60% clay) scenarios; see Table 2 for a description of the scenarios.

7

8

9

10

11

12

13

14



- 1 **Table 1** Summary of scalar parameters used in the non-steady-state (DETECT) model, arranged
- 2 into four groups: parameters unique to the microbial respiration submodel for $S_M(z,t)$ (group 1);
- 3 parameters unique to the root respiration submodel for $S_R(z,t)$ (group 2); parameters that are
- 4 shared between the $S_M(z,t)$ and $S_R(z,t)$ submodels (group 3); parameters used to calculate soil
- 5 CO₂ diffusivity, D_{gs} (group 4).

Symbol	Description	Value	Units	Eqn(s).
Group 1				
R^*	Total root biomass C in a 1 m deep by 1 cm ² soil column	111.5	mg C cm ⁻²	3
R_{RBase}	Root mass-base respiration rate at 10 °C and mean environmental conditions	6×10^{-5}	mg C cm ⁻³ hr ⁻¹	3
$\alpha_{1(R)}$	The effect of soil water content (θ) on root respiration	11.65	unitless	3, 4a
$\alpha_{2(R)}$	The effect of antecedent θ (θ_R^{ant}) on root respiration	20.7	unitless	3, 4b
$\alpha_{3(R)}$	The interactive effect of θ and θ_R^{ant} on root respiration	-164.2	unitless	3, 4c
Group 2				
S^*	Total soil organic C in a 1 meter deep by 1 cm ² soil column	711.6	mg C cm ⁻²	5
M^*	Total microbial biomass C in a 1 meter deep by 1 cm ² column of soil	12.3	mg C cm ⁻²	5
V_{Base}	Value of V_{max} at 10 °C and mean environmental conditions	0.0015	mg C cm ⁻³ hr ⁻¹	5, 6
$\alpha_{1(M)}$	The effect of θ on microbial respiration	14.05	unitless	5, 6
$\alpha_{2(M)}$	The effect of antecedent θ (θ_M^{ant}) on microbial respiration	11.05	unitless	5, 6
$\alpha_{3(M)}$	The interactive effect of θ and θ_M^{ant} on microbial respiration	-87.6	unitless	5, 6
K_m	Michaelis-Menton half saturation constant	10^{-5}	mg C cm ⁻³ hr ⁻¹	5
CUE	Microbial carbon-use efficiency	0.8	mg C / mg C	5
p	Fraction of soil organic C that is soluble	0.004	—	7
D_{liq}	Diffusivity of soil C substrate in liquid	3.17	unitless	7
Group 3				
E_o^*	Temperature sensitivity parameter, somewhat analogous to an energy of activation	324.6	Kelvin	4c
T_o	Temperature sensitivity-related parameter	227.5	Kelvin	4c
α_4	The effect of antecedent soil temperature (T_S^{ant}) on root and microbial respiration	-4.7	unitless	4c
Group 4				
$\alpha_{3(R)}$	Absolute value of the slope of the line relating $\log(\Psi)$ versus $\log(\theta)$	4.547	unitless	2
BD	Soil bulk density	1.12	g cm ⁻³	2
ϕ_{g100}	Air-filled porosity at soil water potential of -100 cm H ₂ O (~10 kPa)	18.16	%	2
PD	Particle density			



- 1 **Table 2** Summary of quantities in the non-steady-state (DETECT) model that vary by depth only
 2 (z), or by depth (z) and time (t). Those in group 1 represent input variables (derived prior to the
 3 running of the DETECT model), while group 2 contains the modeled quantities (used as part of
 4 the operation of the DETECT model). Equation S1 can be found in Appendix S2 in the
 5 supplemental material.

Symbol	Description	Units	Eqn(s).
Group 1			
$f_R(z)$	A function describing the distribution by depth of root carbon.	unitless	S1
$C_R(z, t)$	The amount of root carbon.	mg C cm ⁻³ hr ⁻¹	3, S1
$f_S(z)$	A function describing the distribution by depth of carbon from soil organic matter (SOM)	unitless	S1
$C_{SOM}(z)$	The amount of carbon from SOM.	mg C cm ⁻³ hr ⁻¹	7, S1
$f_M(z)$	A function describing the distribution by depth of microbial carbon	unitless	S1
$C_{MIC}(z)$	The amount of microbial carbon.	mg C cm ⁻³ hr ⁻¹	3, S1
$\theta(z, t)$	Soil water content	m ³ m ⁻³	3, 6, 7
$\theta_R^{ant}(z, t)$	Antecedent soil water content (used in S_R function) calculated as a weighted average of soil water content from the previous 4 days. The weights are $w=(0.75,0.25,0,0)$.	m ³ m ⁻³	3
$\theta_M^{ant}(z, t)$	Antecedent soil water content (used in S_M function) calculated as a weighted average of soil water content from the previous 4 days. The weights are $w=(0.2,0.6,0.2,0)$.	m ³ m ⁻³	6
$T_S(z, t)$	Soil temperature	Kelvin	3, 6
$T_S^{ant}(z, t)$	Antecedent soil temperature calculated as a weighted average of soil temperature from the previous 4 weeks. The weights are $w=(0.25,0.25,0.25,0.25)$.	Kelvin	3, 6
Group 2			
$c(z, t)$	Total soil CO ₂ .	mg CO ₂ m ⁻³	1
$c_r(z, t)$	Soil CO ₂ derived from root sources.	mg CO ₂ m ⁻³	1
$S_r(z, t)$	Source term describing the production of soil CO ₂ from root respiration.	mg CO ₂ m ⁻³	1
$c_m(z, t)$	Soil CO ₂ derived from microbial sources.	mg CO ₂ m ⁻³	1
$S_m(z, t)$	Source term describing the production of soil CO ₂ from microbial respiration.	mg CO ₂ m ⁻³	1
$D_{gs}(z, t)$	Diffusivity of soil CO ₂	m ² s ⁻¹	1, 2
$\phi_g(z, t)$	Air-filled soil porosity.	m ³ m ⁻³	1, 2
$C_{SOL}(z, t)$	The amount of soluble carbon from SOM.	mg C cm ⁻³ hr ⁻¹	5, 7
$V_{max}(z, t)$	Maximum potential decomposition rate (microbial carbon).	mg C cm ⁻³ hr ⁻¹	6
$E_o(z, t)$	Analogous to energy of activation.	Kelvin	4c

6



7 **Table 3** The scenario code, description, and summary of results associated with each model scenario; the 14 scenarios below were
 8 applied to both the DETECT and SS-DETECT models. The scenarios involved a non-factorial combination of different soil texture,
 9 precipitation regimes, and inclusion/exclusion of antecedent effects on the root and microbial CO₂ production rates.

Scenario	Description	Primary result(s)
Scenarios that assume no antecedent effects		
<i>Ctrl</i> (control)	Uses soil texture (sandy clay loam: 60% sand, 20% clay) and precipitation (for 2008) data from the PHACE site; CO ₂ production only responds to concurrent environmental conditions.	R_{soil} was very similar under SS and NSS soil CO ₂ assumptions.
Soil texture scenarios		
<i>ST-Sa</i>	Same as <i>Ctrl</i> , but the soil texture is set to sandy loam (80% sand, 10% clay).	For <i>ST-Cl</i> , R_{soil} was greater in magnitude and more different under SS vs NSS conditions, due to NSS conditions producing greater R_{soil} after a major precipitation event. The results are similar, but muted, for the <i>ST-Si</i> scenario.
<i>ST-Si</i>	Same as <i>Ctrl</i> , but the soil texture is set to silt loam (20% sand, 20% clay).	
<i>ST-Cl</i>	Same as <i>Ctrl</i> , but the soil texture is set to clay (20% sand, 60% clay).	
Precipitation scenarios		
<i>P-E</i>	Same as <i>Ctrl</i> , but daily precipitation was shifted to occur one month earlier.	Varying the timing or magnitude of precipitation pulses had little effect on the magnitude of R_{soil} or on the difference between SS and NSS predictions of R_{soil} .
<i>P-L</i>	Same as <i>Ctrl</i> , but daily precipitation was shifted to occur one month later.	
<i>P-FM</i>	Same as <i>Ctrl</i> , but daily precipitation was based on data from 2009, which is characterized by more frequent, smaller events.	
Scenarios that incorporate antecedent effects on CO₂ production rates		
<i>Ctrl-ant</i> <i>ST-Sa-ant</i> <i>ST-Si-ant</i> <i>ST-Cl-ant</i> <i>P-E-ant</i> <i>P-L-ant</i> <i>P-FM-ant</i>	All scenarios parallel those described about, except both current and antecedent conditions (past soil water and past soil temperature) are used in the calculation of the source terms (i.e., root and microbial CO ₂ production rates).	R_{soil} was generally greater in magnitude under both SS and NSS conditions, especially for <i>ST-Si-ant</i> and <i>ST-Cl-ant</i> (relative to <i>ST-Si</i> and <i>ST-Cl</i>).

10